On the Moreau–Jean scheme with the Frémond impact law: energy conservation and dissipation properties for elastodynamics with contact, impact and friction

Vincent Acary, Nicholas Anton Collins-Craft

On the Moreau–Jean scheme with the Frémond impact law: energy conservation and dissipation properties for elastodynamics with contact, impact and friction

V. Acary* and N.A. Collins-Craft†

April 26, 2024

Highlights A time-stepping scheme with contact, impact and Coulomb friction with

1. the Frémond approach for the Newton impact law with friction; and
2. a discrete energy balance that has positive dissipation;

Keywords contact dynamics, impact, computational contact mechanics, numerical time integration, energy conservation, dissipation properties

Abstract The objective of this paper is to propose a time integration scheme for nonsmooth mechanical systems involving one-sided contact, impact and Coulomb friction, that respects the principles of discrete-time energy balance with positive dissipation. To obtain energetic consistency in the continuous time model when an impact occurs, we work with an impact law with friction inspired by the work of M. Frémond (Frémond, 1995, 2001, 2002, 2017) which ensures that dissipation is positive, *i.e.* that the Clausius–Duhem inequality is satisfied for the impulses and the velocity jumps. On this basis, we propose a time integration method based on the Moreau–Jean scheme (Jean and Moreau, 1987; Moreau, 1988) with a discrete version of the Frémond impact law, and show that this method has correct dissipation properties.

Contents

1 Introduction and motivations **2**

2 Nonsmooth mechanical systems with unilateral contact, Coulomb's friction and impact **3**
2.1 Smooth equations of motion for linear viscoelasticity and constitutive laws . . . 3
2.2 Nonsmooth dynamics . . . 5
2.3 Energy balance analysis . . . 6
2.4 Frémond's model of frictional impact . . . 7

3 Moreau–Jean scheme with discrete Frémond's impact law **8**
3.1 Flaws in the standard Moreau–Jean scheme with Newton's impact law and Coulomb's friction . . . 8
3.2 Principles of the proposed scheme . . . 9
3.3 Discrete dissipation properties and energy balance . . . 10

4 Implementation details in Siconos **11**
4.1 Implementation of the Moreau–Jean scheme . . . 11
4.2 Implementation of the new Moreau–Jean scheme . . . 12

5 Numerical illustrations **12**
5.1 Impacting stick . . . 12
5.2 A rocking block . . . 16
5.3 A sliding block . . . 19
5.4 Impact on masonry structure . . . 23

6 Conclusion **28**

*Centre Inria de l'Université Grenoble Alpes, 655 avenue de l'Europe, 38330 Montbonnot, France.
†Centre Inria de l'Université Grenoble Alpes, 655 avenue de l'Europe, 38330 Montbonnot, France.

Notation The following notation is used throughout the paper. The Euclidean norm for a vector $x \in \mathbb{R}^n$ is denoted by $\|x\|$. For two vectors $x, y \in \mathbb{R}^n$, the Hadamard product is denoted by $x \circ y$. For a positive definite (respectively positive semi-definite) matrix $M \in \mathbb{R}^{n \times n}$, $\|x\|_M$ denotes the norm (respectively the semi-norm) in the metric defined by M. Let I denote a real time interval of any sort. For a function $f : I \to \mathbb{R}^n$ of Bounded Variation (BV), we denote the right-limit function by $f^+(t) = \lim_{s \to t, s > t} f(s)$, and respectively the left-limit by $f^-(t) = \lim_{s \to t, s < t} f(s)$. We denote by $0 = t_0 < t_1 < \ldots < t_k < \ldots < t_N = T$ a finite partition (or a subdivision) of the time interval $[0, T]$, where $(T > 0)$. The integer N is the number of time intervals in the subdivision. The length of a time step is denoted by $h_k = t_{k+1} - t_k$. For simplicity's sake, the schemes are presented in the following with a time step denoted by h for short. The value of a real function $x(t)$ at the time t_k, is approximated by x_k. In the same way, the notation $x_{k+\theta} = (1 - \theta)x_k + \theta x_{k+1}$ is used for $\theta \in [0, 1]$. The notation $\mathrm{d}t$ defines the Lebesgue measure on $\mathbb{R}$.

1 Introduction and motivations

The objective of this paper is to propose a time integration scheme for nonsmooth mechanical systems involving one-sided contact, impact and Coulomb friction, that respects the principles of discrete-time energy balance with positive dissipation. For simplicity, we consider systems either discrete or spatially discretised (by the finite element method (FEM) for example), and that have dynamics that are linear, but with possible nonlinear constraints that model contact. The question of developing a consistent integration scheme with correct energy and dissipation properties implies that the continuous-time model also has these properties. It is known that discrete systems with Coulomb friction and a kinematic impact law can generate energy, in particular, when the direction of sliding velocity changes during impact (Brogliato, 2016; Glocker, 2013). In this work, we therefore propose to work with an impact law inspired by the work of M. Frémond (Frémond, 1995, 2001, 2002, 2007, 2017) which ensures that dissipation is positive, *i.e.* that the Clausius–Duhem inequality (and therefore the second law of thermodynamics) is satisfied. The main ingredient is the use of the average of the pre- and post-impact velocities as the primary kinematic variable conjugated with the impulse. This duality pairing is natural for discrete systems when an impact occurs. The Coulomb law is written with this average velocity. In this way, the work of the contact impulses is always non positive. When the velocity is continuous, the model reverts to the standard one-sided contact model with Coulomb friction. On this basis, we propose a time integration method based on the Moreau–Jean scheme (Jean and Moreau, 1987; Moreau, 1988) and show that this method has good dissipation properties.

Much work in the literature has focused on conservative or energy-dissipating time integration schemes for frictionless one-sided contact systems. These studies are mainly interested in this property because it confers stability properties to the schemes, which are often difficult to obtain. A review of the literature can be found in Acary (2016). On the other hand, there is comparatively little work on contact with Coulomb friction. This may be due to the inherent difficulty of Coulomb friction for discrete systems that exhibit impulses. Amongst the work that has been conducted in the context of variational discrete integrators, we may note the article of Fetecau et al. (2003), who briefly consider the case of friction in the continuous-time case, but do not consider it in their discrete algorithm (which in any case requires the precise location of impacts in time, rendering it infeasible for applications with many impacts such as granular flows). The autonomous case for rigid body dynamics has been treated by Johnson et al. (2014), who allow a frictional impulse over a time step to be sufficiently large to cause the contact to stick (but no larger), thus avoiding any change of sliding direction. However, in the general case of nonautonomous mechanical systems (those with externally imposed driving forces or displacements), and when there are interactions with elasticity and damping, changes in the sliding direction may simply be imposed at the contact, regardless of any interaction with frictional forces. Capobianco and Eugster (2018) consider such a system, and develop an integration scheme that preserves a principle of virtual action, but this does not in itself imply no generation of energy during sliding, only that any energy that is created will be compensated elsewhere in the action. In light of these previous works, there would seem to be considerable interest in ensuring that numerical schemes that are event-capturing (that is to say that do not require the precise location in time of each impact event) are able to remain dissipative, regardless of the nature (elastic, rigid *etc*) of the contacting bodies, and the presence of any external forcing.

The structure of the article is as follows. We begin in Section 2 by presenting the equations of motion of a spatially discrete system with one-sided constraints, Coulomb friction and impacts. After a discussion of the energy balance of the system, we find that the system with Newton's law of impact and Coulomb friction can be non-dissipative. Finally, we propose an impact model inspired by the work of Frémond which guarantees that the system is dissipative. In Section 3, we propose a new scheme that is dissipative in discrete time, with dissipative terms that are numerical approximations of frictional and impact dissipation. In Section 4, we describe how the schemes are implemented in practice in the Siconos software framework. In Section 5, the dissipation properties of the discrete time scheme are illustrated with various examples and compared to the classical Moreau–Jean scheme. Section 6 concludes the article and outlines some perspectives.

2 Nonsmooth mechanical systems with unilateral contact, Coulomb's friction and impact

In this section we consider systems that are continuous in time but discrete in space, and outline the equations of motion and energy balance with Coulomb friction and impact for the standard model and the Frémond impact model.

2.1 Smooth equations of motion for linear viscoelasticity and constitutive laws

The equations of motion of a discrete or discretised Lagrangian mechanical system in the linear visco-elastic case are

$$\begin{cases} q(t_0) = q_0,\ v(t_0) = v_0, & \text{(1a)} \\ \dot{q}(t) = v(t), & \text{(1b)} \\ M\dot{v}(t) + Kq(t) + Cv(t) = F(t) + R(t), & \text{(1c)} \end{cases}$$

where $q(t) \in \mathbb{R}^n$ is the vector of generalised coordinates and $v(t) = \dot{q}(t)$ is the corresponding vector of generalised velocities, the initial conditions are $q_0 \in \mathbb{R}^n$ and $v_0 \in \mathbb{R}^n$, $M \in \mathbb{R}^{n\times n}$ is the symmetric mass matrix that is assumed to be positive definite, $K \in \mathbb{R}^{n\times n}$ is the positive semi-definite stiffness matrix and $C \in \mathbb{R}^{n\times n}$ the positive semi-definite damping matrix, $F(t)$ is the vector of external applied forces and $R(t)$ is the vector of generalised contact forces. The system is now subjected to a finite set of m unilateral contacts that defines the admissible set for the configuration

$$\mathcal{C} = \{q \in \mathbb{R}^n \mid g_{\text{N}}^\alpha(q) \geqslant 0, \alpha \in [\![1, m]\!]\} \subset \mathbb{R}^n, \tag{2}$$

where $g_{\text{N}}^\alpha : \mathbb{R}^n \to \mathbb{R}$ is assumed to be a smooth function with non-vanishing gradients. We denote by the function $g_{\text{N}} : \mathbb{R}^n \to \mathbb{R}^m$ the function with g_{N}^α as components. For the perfect unilateral constraints, the Signorini condition is written as

$$0 \leqslant g_{\text{N}}(q(t)) \perp \lambda(t) \geqslant 0, \tag{3}$$

where the inequalities involving vectors are understood to hold component-wise and the $\perp$ symbol means that $g_{\text{N}}^\top \lambda = 0$. The Lagrange multiplier λ is related to the generalised reaction force R by

$$R(t) = \nabla_q g_{\text{N}}(q(t))\lambda(t). \tag{4}$$

The Signorini condition at the velocity level can be also be defined as

$$0 \leqslant u_{\text{N}}(t) \perp \lambda(t) \geqslant 0, \text{ if } g_{\text{N}}(q(t)) \leqslant 0, \tag{5}$$

where the local relative velocity $u_{\text{N}}(t)$ is defined by

$$u_{\text{N}}(t) = \dot{g}(q(t)) = \nabla_q^\top g_{\text{N}}(q(t))\, v(t). \tag{6}$$

Moreau's viability lemma ensures that (5) implies (3) if the initial conditions are admissible.

Coulomb friction For Coulomb friction, the definition of the gradients of the constraints is not sufficient and an orthonormal local basis $(\mathsf{n}^\alpha, \mathsf{t}_1^\alpha, \mathsf{t}_2^\alpha)$ at contact composed of the inward normal vector $n^\alpha \in \mathbb{R}^3$ to set $\mathcal{C}$ and the tangential vectors $\mathsf{t}_1^\alpha, \mathsf{t}_2^\alpha \in \mathbb{R}^3$ is needed. For an individual contact α, the relative velocity and the reaction force r at contact are denoted in this local contact frame as

$$u^\alpha = \begin{pmatrix} u_{\text{N}}^\alpha \\ u_{\text{T}}^\alpha \end{pmatrix}, \quad r^\alpha = \begin{pmatrix} r_{\text{N}}^\alpha \\ r_{\text{T}}^\alpha \end{pmatrix}, \tag{7}$$

where $u_{\text{N}}^\alpha \in \mathbb{R}$, $u_{\text{T}}^\alpha = \begin{pmatrix} u_{\text{T}_1}^\alpha, & u_{\text{T}_2}^\alpha \end{pmatrix}^\top \in \mathbb{R}^2$, $r_{\text{N}}^\alpha \in \mathbb{R}$ and $r_{\text{T}}^\alpha = \begin{pmatrix} r_{\text{T}_1}^\alpha, & r_{\text{T}_2}^\alpha \end{pmatrix}^\top \in \mathbb{R}^2$. The local variables are related to the generalised variables by

$$u^\alpha = H^\alpha(q)\, v, \quad R^\alpha = H^{\alpha,\top}(q)\, r^\alpha. \tag{8}$$

Coulomb friction together with the Signorini condition at the velocity level is given by

$$-\tilde{u}^\alpha \in N_{\mathcal{K}^\alpha}(r^\alpha), \quad \text{if } g_{\text{N}}^\alpha(q) \leqslant 0, \text{ else } r^\alpha = 0 \tag{9}$$

where $\tilde{u}$ is the modified De Saxcé velocity expressed as

$$\tilde{u}^\alpha = u^\alpha + \begin{pmatrix} \mu^\alpha \|u_{\text{T}}^\alpha\| \\ 0 \\ 0 \end{pmatrix}, \tag{10}$$

and $\mathcal{K}^\alpha$ is the Coulomb cone

$$\mathcal{K}^\alpha = \{r, \|r_{\text{T}}\| \leqslant \mu^\alpha r_{\text{N}}\}, \tag{11}$$

with $\mu^\alpha \geqslant 0$ the friction coefficient. Let $\mathcal{I} = [\![1, m]\!] \in \mathbb{N}$ be the set of indices of constraints. Let us define now the index of constraint at the velocity level by

$$\mathcal{I}^1 = \{\alpha \in \mathcal{I} \mid g_{\text{N}}^\alpha(q(t)) \leqslant 0\}. \tag{12}$$

By collecting all the variables for each contact in the set $\mathcal{I}^1$, and implicitly introducing the notation dropping α ($x = [x^{\alpha,\top}, \alpha \in \mathcal{I}^1]^\top$), we get for the frictional contacts

$$-\tilde{u} \in \text{N}_{\mathcal{K}}(r), \tag{13}$$

considering that $r^\alpha = 0$ for $\alpha \notin \mathcal{I}^1$ and $\mathcal{K}$ is the Cartesian product of the cone $\mathcal{K}^\alpha$. Using the dual cone of $\mathcal{K}$ denoted by

$$\mathcal{K}^\star = \{u, \mu\|u_{\text{T}}\| \leqslant u_{\text{N}}\}, \tag{14}$$

the relation (13) can be written as

$$-r \in \text{N}_{\mathcal{K}^\star}(\tilde{u}). \tag{15}$$

or as a complementarity condition

$$\mathcal{K}^\star \ni \tilde{u} \perp r \in \mathcal{K}. \tag{16}$$

To be self-contained, the equivalence with the standard form of the Coulomb friction is given in the following Lemma 1.

Lemma 1 (Acary et al. (2011)) *For one contact point, the Coulomb friction law with the Signorini condition at the velocity level fulfils one of the three following conditions:*

$$\begin{cases} \textit{either} & r = 0 \textit{ and } u_N \geqslant 0, & \textit{(take-off)} \\ \textit{or} & u = 0 \textit{ and } \|r_T\| \leqslant \mu r_N, & \textit{(sticking)} \\ \textit{or} & \|r_T\| = \mu r_N \textit{ and } u_N = 0 \textit{ and } \|u_T\| r_T = -\|r_T\| u_T, & \textit{(sliding)} \end{cases} \tag{17}$$

and is equivalent to the complementarity problem

$$\mathcal{K}^\star \ni \tilde{u} \perp r \in \mathcal{K}, \tag{18}$$

with

$$\tilde{u} = u + \begin{pmatrix} \mu\|u_T\| \\ 0 \\ 0 \end{pmatrix}. \tag{19}$$

Proof ($\Longrightarrow$) The conditions (17) imply that $r \in \mathcal{K}$ and $u_{\text{N}} \geqslant 0$. Then $\tilde{u}_{\text{N}} \geqslant \mu\|u_{\text{T}}\|$ and we conclude that $\tilde{u} \in \mathcal{K}^\star$. If $u = 0$, then $\tilde{u} = 0$ and the relation $\tilde{u}^\top r = 0$ holds trivially. The same applies for $r = 0$. In the sliding case, we have

$$\tilde{u}^\top r = (u_{\text{N}} + \mu\|u_{\text{T}}\|) r_{\text{N}} + u_{\text{T}}^\top r_{\text{T}} = \|u_{\text{T}}\| \|r_{\text{T}}\| + u_{\text{T}}^\top r_{\text{T}} \tag{20}$$

since $u_{\text{N}} = 0$ and $\mu r_{\text{N}} = \|r_{\text{T}}\|$. Furthermore $\|u_{\text{T}}\| r_{\text{T}} = -\|r_{\text{T}}\| u_{\text{T}}$, the vectors u_{T} and r_{T} are collinear and have opposite directions, we have $u_{\text{T}}^\top r_{\text{T}} = -\|u_{\text{T}}\| \|r_{\text{T}}\|$ and hence $\tilde{u}^\top r = 0$.

($\Longleftarrow$) Conversely, if (18) holds, we have three separate cases:

1. $r = 0$. The relation $\tilde{u} \in \mathcal{K}^\star$ holds. This implies $u_{\text{N}} \geqslant 0$. We have the take-off case.
2. $\tilde{u} = 0$. This implies that $u = 0$ and we have $r \in \mathcal{K}$. Hence, we have the sticking case.
3. $\tilde{u} \neq 0$ and $r \neq 0$. Using $\tilde{u} \in \mathcal{K}^\star$ and $r \in \mathcal{K}$, we get

$$\mu\|\tilde{u}_{\text{T}}\| \|r_{\text{T}}\| \leqslant \mu \tilde{u}_{\text{N}} = r_{\text{N}}. \tag{21}$$

The relation $\tilde{u}^\top r = 0$ implies $\tilde{u}_{\text{N}} r_{\text{N}} = -\tilde{u}_{\text{T}}^\top r_{\text{T}}$ so we get

$$\mu\|\tilde{u}_{\text{T}}\| \|r_{\text{T}}\| \leqslant -\mu \tilde{u}_{\text{T}}^\top r_{\text{T}}. \tag{22}$$

The Cauchy–Schwarz inequality gives

$$\mu\|\tilde{u}_{\text{T}}\| \|r_{\text{T}}\| \geqslant -\mu \tilde{u}_{\text{T}}^\top r_{\text{T}}, \tag{23}$$

so we conclude that

$$\mu\|\tilde{u}_{\text{T}}\| \|r_{\text{T}}\| = -\mu \tilde{u}_{\text{T}}^\top r_{\text{T}}. \tag{24}$$

When $\mu \neq 0$, the vectors $\tilde{u}_{\text{T}}$ and r_{T} are collinear and have the opposite direction to each other, since the Cauchy–Schwarz inequality holds as an equality. Let us assume that $r \in \text{int}(\mathcal{K})$, then $\|r_{\text{T}}\| < \mu r_{\text{N}}$. Since $u \in \mathcal{K}^\star$, we have

$$\mu\|\tilde{u}_{\text{T}}\| \|r_{\text{T}}\| < \mu r_{\text{N}} \tilde{u}_{\text{N}} = -\mu \tilde{u}_{\text{T}}^\top r_{\text{T}}, \tag{25}$$

which contradicts (24). Hence, we conclude $r \in \partial\mathcal{K}$ and hence $\|r_{\text{T}}\| = \mu r_{\text{N}}$. Let us assume that $\tilde{u} \in \text{int}(\mathcal{K}^\star)$, then $\mu\|\tilde{u}_{\text{T}}\| < \tilde{u}_{\text{N}}$. Since $r \in \mathcal{K}$, $\mu\|\tilde{u}_{\text{T}}\| \|r_{\text{T}}\| < \mu r_{\text{N}} \tilde{u}_{\text{N}}$ contradicts (24). Hence, we conclude $\tilde{u} \in \partial\mathcal{K}^\star$. From $\tilde{u} \in \partial\mathcal{K}^\star$, we conclude that $u_{\text{N}} = 0$. □

Smooth dynamics with Coulomb friction For the sake of simplicity, we note by

$$-\tilde{u} = \Phi(u) \tag{26}$$

the De Saxcé change of variable defined in (10) for a given contact α. The smooth dynamics with Coulomb friction is then given by

$$\begin{cases} q(t_0) = q_0,\ v(t_0) = v_0, & \text{(27a)} \\ \dot{q}(t) = v(t), & \text{(27b)} \\ M\dot{v}(t) + Kq(t) + Cv(t) = F_{\text{ext}}(t) + H^\top(q(t))r(t), & \text{(27c)} \\ u(t) = H(q(t))v(t), & \text{(27d)} \\ -\Phi(u) \in \mathrm{N}_{\mathcal{K}}(r). & \text{(27e)} \end{cases}$$

2.2 Nonsmooth dynamics

If a contact α is closing at time t_i with a negative relative velocity, that is $g_{\mathrm{N}}^\alpha(q(t_i)) = 0$ and $u_{\mathrm{N}}^\alpha(t_i) < 0$, we have an impact at t_i. The velocity must jump to satisfy the unilateral constraint immediately after the impact $g_{\mathrm{N}}^\alpha(q(t_i + \varepsilon)) \geqslant 0, \varepsilon > 0$. The velocity v is usually assumed to be a function of bounded variations. The same applies for the relative velocity at contact. With finite dimensional systems, the smooth dynamics (27) are generally insufficient to characterise the solution (that is to say that there are infinitely many solutions after impacts). To close the system at the impact time t_i when $v^+(t_i) \neq v^-(t_i)$, an impact law must be added. In this work, we consider Newton's impact law:

$$u_{\mathrm{N}}^{\alpha,+}(t_i) = -e^\alpha u_{\mathrm{N}}^{\alpha,-}(t_i) \text{ if } g_{\mathrm{N}}^\alpha(q(t_i)) \leqslant 0 \text{ and } u_{\mathrm{N}}^{\alpha,-}(t_i) \leqslant 0, \tag{28}$$

where $e^\alpha \in [0,1]$ is the Newton coefficient of restitution. To address the case of multiple contacts, the Newton impact law is extended in terms of complementarity by Moreau (1988) as

$$0 \leqslant u_{\mathrm{N}}^{\alpha,+}(t_i) + e^\alpha u_{\mathrm{N}}^{\alpha,-}(t_i) \perp p_i^\alpha \geqslant 0, \text{ if } \alpha \in \bar{\mathcal{I}}^1, \tag{29}$$

where p_i is the reaction impulse at time t_i and $\bar{\mathcal{I}}^1$ is the index set defined by

$$\bar{\mathcal{I}}^1 = \{\alpha \in \mathcal{I} \mid g_{\mathrm{N}}^\alpha(q(t)) \leqslant 0 \text{ and } u_{\mathrm{N}}^{\alpha,-}(t) \leqslant 0\}. \tag{30}$$

In the following, we will assume that the local variables at contact are collected for all indices belonging to $\bar{\mathcal{I}}^1$.

The nonsmooth equations of motion are written in terms of differential measure $\mathrm{d}v$ associated with v and the local impulse measure $\mathrm{d}i$ as follows

$$\begin{cases} q(t_0) = q_0,\ v^-(t_0) = v_0, & \text{(31a)} \\ \dot{q} = v, & \text{(31b)} \\ M\,\mathrm{d}v + Kq\,\mathrm{d}t + Cv\,\mathrm{d}t = F\,\mathrm{d}t + H^\top(q)\,\mathrm{d}i, & \text{(31c)} \\ u = H(q)v, & \text{(31d)} \\ -\Psi(u^+) \in \mathrm{N}_{\mathcal{K}}(\mathrm{d}i), & \text{(31e)} \end{cases}$$

where we have made use of the following function that takes into account the impact law (29):

$$\Psi^\alpha(u^\alpha) = u^\alpha + \begin{pmatrix} \mu\|u_{\mathrm{T}}^\alpha\| + e^\alpha u_{\mathrm{N}}^{\alpha,-} \\ 0 \\ 0 \end{pmatrix}. \tag{32}$$

Interpretation of the contact law (31e) **in terms of measures** The equation (31e) requires some explanation based on the definition of a normal cone inclusion with measures. Almost everywhere with respect to the Lebesgue measure $\mathrm{d}t$, we have

$$-\Psi(u^+) \in \mathrm{N}_{\mathcal{K}}(r), \tag{33}$$

where r is the density of $\mathrm{d}i$ with respect to $\mathrm{d}t$. Since we have $u^- = u^+ = u$ almost everywhere, the relation (33) can be written for a contact α as

$$\bar{u}^\alpha = \begin{pmatrix} (1+e^\alpha)u_{\mathrm{N}}^\alpha + \mu\|u_{\mathrm{T}}^\alpha\| \\ u_{\mathrm{T}}^\alpha \end{pmatrix} \in \mathrm{N}_{\mathcal{K}^\alpha}(r^\alpha), \tag{34}$$

Three cases are possible following the proof of the Lemma 1:

1. The take-off case: $r^\alpha = 0$. In that case, we have $u_{\mathrm{N}}^\alpha \geqslant 0$.
2. The sticking case: $\bar{u}^\alpha = 0$. In that case, we have $u_{\mathrm{T}}^\alpha = 0$ and $(1+e^\alpha)u_{\mathrm{N}}^\alpha = 0 = u_{\mathrm{N}}^\alpha$ and $r^\alpha \in \mathcal{K}^\alpha$.

3. The sliding case: $r^\alpha \neq 0$ and $\bar{u}^\alpha \neq 0$. Then we have $r^\alpha \in \partial\mathcal{K}^\alpha$ and $\bar{u}^\alpha \in \partial\mathcal{K}^{\alpha,\star}$. This implies $(1+e)u_{\mathrm{N}}^\alpha = 0 = u_{\mathrm{N}}^\alpha$, $\|r_{\mathrm{T}}\| = \mu r_{\mathrm{N}}$ and $\|u_{\mathrm{T}}\| r_{\mathrm{T}} = -\|r_{\mathrm{T}}\| u_{\mathrm{T}}$.

To conclude, we retrieve almost everywhere the Coulomb friction with the Signorini condition at the velocity level. At any time t_i, we have

$$-\Psi(u^+) \in \mathrm{N}_{\mathcal{K}}(p_i), \tag{35}$$

where p_i is the density of $\mathrm{d}i$ with respect to the Dirac atom at t_i, δ_{t_i}. Once again, we have three possible cases for a contact α:

1. The take-off case: $p_i^\alpha = 0$. In this case, we have $u_{\mathrm{N}}^{\alpha,+} + e u_{\mathrm{N}}^{\alpha,-} \geqslant 0$.
2. The sticking case: $\Psi(u^{\alpha,+}) = 0$. In this case, we have $u_{\mathrm{T}}^{\alpha,+} = 0$ and $u_{\mathrm{N}}^{\alpha,+} + e u_{\mathrm{N}}^{\alpha,-} = 0$ and $p_i^\alpha \in \mathcal{K}^\alpha$. The impact law is satisfied since $u_{\mathrm{N}}^{\alpha,+} = -e u_{\mathrm{N}}^{\alpha,-}$
3. The sliding case: $p_i^\alpha \neq 0$ and $\Psi(u^{\alpha,+}) \neq 0$. Then we have $p_i^\alpha \in \partial\mathcal{K}^\alpha$ and $\Psi(u^{\alpha,+}) \in \partial\mathcal{K}^{\alpha,\star}$. This implies $u_{\mathrm{N}}^{\alpha,+} + e u_{\mathrm{N}}^{\alpha,-} = 0$, $\|p_{i,\mathrm{T}}^\alpha\| = \mu p_{i,\mathrm{N}}^\alpha$ and $\|u_{\mathrm{T}}^{\alpha,+}\| p_{i,\mathrm{T}}^\alpha = -\|p_{i,\mathrm{T}}^\alpha\| u_{\mathrm{T}}^{\alpha,+}$.

To summarise, the impact law is satisfied in the sticking and sliding cases and the Coulomb friction is written in terms of impulses and of the right limit of the relative velocity. We will see in the following that these choices have a consequence for the dissipativity of the model.

2.3 Energy balance analysis

A detailed analysis of the energy balance for nonsmooth systems can be found in Lozano et al. (2013) and Leine and Wouw (2008). The energy balance is usually obtained by multiplying the equation of motion by $v^+ + v^-$. After some algebraic manipulations (see Acary (2016)), we obtain

$$2\,\mathrm{d}\mathcal{E} = \mathrm{d}(v^\top M v) + 2 q^\top K\,\mathrm{d}q = 2 v^\top F\,\mathrm{d}t - 2 v^\top C v\,\mathrm{d}t + (v^+ + v^-)^\top H^\top(q)\,\mathrm{d}i, \tag{36}$$

where the standard definition of the total mechanical energy of the system is

$$\mathcal{E} = \frac{1}{2} v^\top M v + \frac{1}{2} q^\top K q, \tag{37}$$

and $\mathrm{d}q = v^+(t)\,\mathrm{d}t = v^-(t)\,\mathrm{d}t$.

Energy balance almost everywhere Almost everywhere with respect to the Lebesgue measure $\mathrm{d}t$, the energy balance (36) is

$$\frac{\mathrm{d}}{\mathrm{d}t}\mathcal{E}(t) = v^\top(t) F(t) - v^\top(t) C v(t) + v^\top(t) H^\top(q(t)) r(t), \tag{38}$$

which is the classical energy balance for a smooth dynamical system subjected to some constraints. The term $v^\top F$ is the power of the external forces and $-v^\top C v$ is the power of the viscous forces. The last term corresponds to the power of the reaction forces. For a contact α, it can be decomposed as

$$v^\top H^{\alpha,\top}(q) r^\alpha = u^{\alpha,\top} r^\alpha = u_{\mathrm{N}}^\alpha r_{\mathrm{N}}^\alpha + u_{\mathrm{T}}^{\alpha,\top} r_{\mathrm{T}}^\alpha. \tag{39}$$

As we assumed that the constitutive law (33) is satisfied almost everywhere, an examination of the three possibles cases for the contact law yields

$$v^\top H^{\alpha,\top}(q) r^\alpha = -\mu^\alpha r_{\mathrm{N}}^\alpha \|u_{\mathrm{T}}^\alpha\|, \tag{40}$$

which is the standard dissipated power by a sliding contact with Coulomb friction. Note that the dissipated power is always non-positive, which is consistent with the laws of thermodynamics.

Energy balance at any time At any time t_i, the energy balance (36) is

$$\mathcal{E}^+(t_i) - \mathcal{E}^-(t_i) = \frac{1}{2}(v^+(t_i) + v^-(t_i))^\top H^\top(q(t_i)) p_i. \tag{41}$$

For a contact α, it can be evaluated as

$$\frac{1}{2}(v^+(t_i) + v^-(t_i))^\top H^{\alpha,\top}(q(t_i)) p_i^\alpha = \frac{1}{2}(u^{\alpha,+}(t_i) + u^{\alpha,-}(t_i))^\top p_i^\alpha. \tag{42}$$

With the constitutive law given by (33), the dissipated power in (42) vanishes in the take-off case. In the sticking case, the sliding velocity vanishes and we get

$$\begin{aligned}\frac{1}{2}(v^+(t_i) + v^-(t_i))^\top H^{\alpha,\top}(q(t_i)) p_i^\alpha &= \frac{1}{2}(u_{\mathrm{N}}^{\alpha,+}(t_i) + u_{\mathrm{N}}^{\alpha,-}(t_i)) p_{\mathrm{N},i}^\alpha + \frac{1}{2} u_{\mathrm{T}}^{\alpha,-}(t_i) p_{\mathrm{T},i}^\alpha, \\ &= \frac{1}{2}(1-e) u_{\mathrm{N}}^{\alpha,-}(t_i) p_{\mathrm{N},i}^\alpha + \frac{1}{2} u_{\mathrm{T}}^{\alpha,-}(t_i) p_{\mathrm{T},i}^\alpha.\end{aligned} \tag{43}$$

Since $u_{\mathrm{N}}^{\alpha,-}(t_i) \leqslant 0$ and $e \in [0,1]$, the first term of the dissipated power by an impact is non-positive, but we cannot conclude *a priori* on the sign of the second term. In the sliding case, we get

$$\begin{aligned}\frac{1}{2}(v^+(t_i)+v^-(t_i))^\top H^{\alpha,\top}(q(t_i))p_i^\alpha &= \frac{1}{2}(1-e)u_{\mathrm{N}}^{\alpha,-}(t_i)p_{\mathrm{N},i}^\alpha + \frac{1}{2}(u_{\mathrm{T}}^{\alpha,+}(t_i)+u_{\mathrm{T}}^{\alpha,-}(t_i))^\top p_{\mathrm{T},i}^\alpha,\\ &= \frac{1}{2}(1-e)u_{\mathrm{N}}^{\alpha,-}(t_i)p_{\mathrm{N},i}^\alpha - \frac{1}{2}\mu^\alpha p_{\mathrm{N},i}^\alpha \|u_{\mathrm{T}}^{\alpha,+}(t_i)\| + \frac{1}{2}(u_{\mathrm{T}}^{\alpha,-}(t_i))^\top p_{\mathrm{T},i}^\alpha. \end{aligned} \tag{44}$$

The first two terms in (44) are non-positive. For the last terms, we cannot conclude *a priori* on its sign. For instance, if there is a reversal of the sliding direction during the impact, $u_{\mathrm{T}}^{\alpha,-}(t_i) = -u_{\mathrm{T}}^{\alpha,-}(t_i)$, the power of the frictional impulse may generate energy. In other words, the Coulomb law in terms of impulses together with the Newton impact law is not dissipative and does not respect the second law of thermodynamics.

This fact is not new. The famous Kane (1984) example (see also Brogliato (2016) and Glocker (2013)) shows that some amount of energy can be generated using this type of constitutive law. For our purpose, it would appear to be difficult to propose a consistent numerical scheme that dissipates energy when the underlying law does not possess this property.

2.4 Frémond's model of frictional impact

To obtain a constitutive law that is consistent with the laws of thermodynamics and the Newton impact law, we propose to use

$$-\Xi\left(\frac{1}{2}(u^+ + u^-)\right) \in \mathrm{N}_{\mathcal{K}}(\mathrm{d}i) \tag{45}$$

with

$$\Xi^\alpha(\bar{u}^\alpha) = \begin{pmatrix} \bar{u}_{\mathrm{N}}^\alpha + \frac{1}{2}(e^\alpha - 1)\bar{u}_{\mathrm{N}}^{\alpha,-} + \mu^\alpha \|\bar{u}_{\mathrm{T}}^\alpha\| \\ \bar{u}_{\mathrm{T}}^\alpha \end{pmatrix} \quad \text{and } \bar{u}^\alpha = \frac{1}{2}(u^{\alpha,+} + u^{\alpha,-}). \tag{46}$$

This law is inspired by the energy balance (42) and the work of Frémond (Frémond, 1995, 2001, 2002, 2017). We will refer to this constitutive law as the Frémond model in the following. We will now demonstrate that the Frémond model always dissipates energy.

Lemma 2 *The Frémond model of contact, impact and friction given by* (45) *and* (46) *satisfies the dissipation inequality, that is*

$$\frac{1}{2}(v^+ + v^-)^\top H^\top(q)\,\mathrm{d}i \leqslant 0. \tag{47}$$

Proof Almost everywhere with respect to the Lebesgue measure $\mathrm{d}t$, we have $u^+ = u^- = u$, and the constitutive law (45) reduces to

$$-\begin{pmatrix} \frac{1}{2}(1+e^\alpha)u_{\mathrm{N}}^\alpha + \mu^\alpha \|u_{\mathrm{T}}^\alpha\| \\ u_{\mathrm{T}}^\alpha \end{pmatrix} \in \mathrm{N}_{\mathcal{K}}(r). \tag{48}$$

The three possible cases of (48) coincide with those of (33). In other words, for the smooth dynamics, there is no difference between the law in (45) and the standard Coulomb law with the Signorini condition at the velocity level given by (33). At any time t_i, we obtain

$$-\Xi\left(\frac{1}{2}\left[u^+(t_i) + u^-(t_i)\right]\right) \in \mathrm{N}_{\mathcal{K}}(p_i). \tag{49}$$

To be explicit, let us examine the three possible cases for a contact α:

1. The take-off case: $p_i^\alpha = 0$. In this case, we have $\frac{1}{2}(u_{\mathrm{N}}^{\alpha,+} + u_{\mathrm{N}}^{\alpha,-}) + \frac{1}{2}(e^\alpha - 1)u_{\mathrm{N}}^{\alpha,-} \geqslant 0$, that is to say $u_{\mathrm{N}}^{\alpha,+} + e u_{\mathrm{N}}^{\alpha,-} \geqslant 0$.
2. The sticking case: $\Xi(\frac{1}{2}[u^{\alpha,+}(t_i) + u^{\alpha,-}(t_i)]) = 0$. In this case, we have $\frac{1}{2}(u_{\mathrm{T}}^{\alpha,+} + u_{\mathrm{T}}^{\alpha,-}) = 0$, $u_{\mathrm{N}}^{\alpha,+} + e u_{\mathrm{N}}^{\alpha,-} = 0$ and $p_i^\alpha \in \mathcal{K}^\alpha$. The impact law is satisfied since $u_{\mathrm{N}}^{\alpha,+} = -e u_{\mathrm{N}}^{\alpha,-}$. Note that in the sticking case, we have $u_{\mathrm{T}}^{\alpha,+} = -u_{\mathrm{T}}^{\alpha,-}$, which may take non-zero values. Only the velocity average over the time of impact vanishes.
3. The sliding case: $p_i^\alpha \neq 0$ and $\Xi(\frac{1}{2}(u^{\alpha,+}(t_i) + u^{\alpha,-}(t_i))) \neq 0$. Then we have $p_i^\alpha \in \partial\mathcal{K}^\alpha$ and $\Xi(\frac{1}{2}[u^{\alpha,+}(t_i) + u^{\alpha,-}(t_i)]) \in \partial\mathcal{K}^{\alpha,\star}$. This implies $u_{\mathrm{N}}^{\alpha,+} + e u_{\mathrm{N}}^{\alpha,-} = 0$, $\|p_{i,\mathrm{T}}^\alpha\| = \mu p_{i,\mathrm{N}}^\alpha$ and $\|\frac{1}{2}(u^+(t_i) + u^-(t_i))\| p_{i,\mathrm{T}}^\alpha = -\|p_{i,\mathrm{T}}^\alpha\| \frac{1}{2}(u^+(t_i) + u^-(t_i))$.

In the take-off case, the impulse p_i vanishes and hence the dissipated power vanishes.

In the sticking case, we obtain

$$\begin{aligned}\frac{1}{2}(v^+(t_i)+v^-(t_i))^\top H^{\alpha,\top}(q(t_i))p_i^\alpha &= \frac{1}{2}(u_{\mathrm{N}}^{\alpha,+}(t_i)+u_{\mathrm{N}}^{\alpha,-}(t_i))p_{\mathrm{N},i}^\alpha,\\ &= \frac{1}{2}(1-e)u_{\mathrm{N}}^{\alpha,-}(t_i)p_{\mathrm{N},i}^\alpha \leqslant 0,\end{aligned} \tag{50}$$

since $\frac{1}{2}(u_{\mathrm{T}}^{\alpha,+}(t_i)+u_{\mathrm{T}}^{\alpha,-}(t_i))$ vanishes. Since $u_{\mathrm{N}}^{\alpha,-}(t_i)\leqslant 0$ and $e\in[0,1]$, the dissipated power by an impact is non-positive.

In the sliding case, we get

$$\begin{aligned}\frac{1}{2}(v^+(t_i)+v^-(t_i))^\top H^{\alpha,\top}(q(t_i))p_i^\alpha &= \frac{1}{2}(1-e)u_{\mathrm{N}}^{\alpha,-}(t_i)p_{\mathrm{N},i}^\alpha + \frac{1}{2}(u_{\mathrm{T}}^{\alpha,+}(t_i)+u_{\mathrm{T}}^{\alpha,-}(t_i))^\top p_{\mathrm{T},i}^\alpha,\\ &= \frac{1}{2}(1-e)u_{\mathrm{N}}^{\alpha,-}(t_i)p_{\mathrm{N},i}^\alpha - \frac{1}{2}\mu^\alpha p_{\mathrm{N},i}^\alpha\|\frac{1}{2}(u_{\mathrm{T}}^{\alpha,+}(t_i)+u_{\mathrm{T}}^{\alpha,-}(t_i))\|\leqslant 0.\end{aligned} \tag{51}$$

□

We conclude that the dissipated power related to the reaction forces is always non-negative. In other words, the model satisfies the laws of thermodynamics at the time of impact. The average of the pre-impact and post-impact velocities $\frac{1}{2}(v^+ + v^-)$ is the natural dual variable of the impulse in the energy balance, or in the principle of virtual power. Choosing a constitutive law that relates this velocity to the impulse though a pseudo-potential of dissipation

$$-p \in \chi_{\mathcal{K}^\star}\left(\Xi\left(\frac{1}{2}[v^+ + v^-]\right)\right) \tag{52}$$

is a way to define a dissipative law (Moreau, 1971, 1973). χ_C is the indicator function of a convex set C, defined by

$$\chi_C(x) = \begin{cases} 0 & \text{if } x\in C,\\ \infty & \text{if } x\notin C.\end{cases} \tag{53}$$

Remark 1 *The model proposed by Frémond is not only consistent with the laws of thermodynamics, but has also been validated by experimental tests. In Cholet (1998) and Frémond (2001, 2002, 2017), we find experimental results showing that percussions belong to the Coulomb cone. Even more interestingly, these experimental tests also show that the Coulomb relationship between impact and velocity is valid for the averaged velocity $\frac{1}{2}(u^+(t_i)+u^-(t_i))$, but not for the velocity after impact $u^+(t_i)$.*

3 Moreau–Jean scheme with discrete Frémond's impact law

3.1 Flaws in the standard Moreau–Jean scheme with Newton's impact law and Coulomb's friction

In this section we consider systems that are discrete in both space and time, demonstrate the problems with the Moreau–Jean scheme and the standard law, and demonstrate that the Moreau–Jean scheme with the Frémond law avoids these problems.

Formulation of the Moreau–Jean scheme The Moreau–Jean scheme (Jean, 1999; Jean and Moreau, 1987; Moreau, 1988) on an interval $(t_k, t_{k+1}]$ of length h is as follows

$$\begin{cases} M(v_{k+1}-v_k)+hKq_{k+\theta}+hCv_{k+\theta}-hF_{k+\theta} = H^\top(q_k)p_{k+1}, & \text{(54a)}\\ q_{k+1} = q_k + hv_{k+\theta}, & \text{(54b)}\\ u_{k+1} = H(q_k)\,v_{k+1}, & \text{(54c)}\\ -\Gamma(u_{k+1})\in \mathrm{N}_{\mathcal{K}}(p_{k+1}) & \text{(54d)}\end{cases}$$

with $\theta\in[0,1]$ and where

$$\Gamma^\alpha(u_{k+1}^\alpha) = u_{k+1}^\alpha + \begin{pmatrix} eu_{\mathrm{N},k}^\alpha + \mu^\alpha\|u_{\mathrm{T},k+1}^\alpha\|\\ 0\\ 0\end{pmatrix}. \tag{55}$$

The following approximations are considered:

$$v_{k+1}\approx v(t_{k+1});\quad u_{k+1}\approx u^+(t_{k+1});\quad p_{k+1}\approx \mathrm{d}i((t_k,t_{k+1}]). \tag{56}$$

The index set $\bar{\mathcal{I}}^1$ is approximated at each time step by

$$\bar{\mathcal{I}}^1_k = \{\alpha \in \mathcal{I} \mid g^\alpha(q_k) \leqslant 0 \text{ and } u^\alpha_{\mathrm{N},k} \leqslant 0\}. \tag{57}$$

The discrete variables at each contact are collected in the unknown variables u_{k+1} and p_{k+1} for the indices such that $\alpha \in \bar{\mathcal{I}}^1_k$.

Discrete dissipation analysis Following Lemma 5.1 in Acary (2016), the discrete-time dissipation equality of the Moreau–Jean scheme (54) over a time-step $[t_k, t_{k+1}]$ is given by

$$\Delta\mathcal{E} - W^{\mathsf{ext}}_{k+1} - W^{\mathsf{damping}}_{k+1} = \left(\frac{1}{2} - \theta\right)\left[\|v_{k+1} - v_k\|^2_M + \|q_{k+1} - q_k\|^2_K\right] + u^\top_{k+\theta} p_{k+1}, \tag{58}$$

and the discrete approximation of the work done by the external forces within the step by

$$W^{\mathsf{ext}}_{k+1} = h v^\top_{k+\theta} F_{k+\theta} \approx \int_{t_k}^{t_{k+1}} F v \,\mathrm{d}t, \tag{59}$$

and the discrete approximation of the work done by the damping term by

$$W^{\mathsf{damping}}_{k+1} = -h v^\top_{k+\theta} C v_{k+\theta} \approx -\int_{t_k}^{t_{k+1}} v^\top C v \,\mathrm{d}t. \tag{60}$$

To ensure that the scheme dissipates energy, the first condition is $\theta \geqslant \dfrac{1}{2}$. The second condition is related to the sign of the discrete work of the reaction impulse given by

$$u^\top_{k+\theta} p_{k+1} = u^\top_{\mathrm{N},k+\theta} p_{\mathrm{N},k+1} + u^\top_{\mathrm{T},k+\theta} p_{\mathrm{T},k+1}. \tag{61}$$

For a contact α, the normal term $u^{\alpha,\top}_{\mathrm{N},k+\theta} p^\alpha_{\mathrm{N},k+1}$ vanishes in the take-off case, and is given by

$$u^{\alpha,\top}_{\mathrm{N},k+\theta} p^\alpha_{\mathrm{N},k+1} = \left[1 - \theta\left(1 + e^\alpha\right)\right] u^\alpha_{\mathrm{N},k} p^\alpha_{\mathrm{N},k+1}, \tag{62}$$

in the sliding and sticking cases. With the condition

$$\theta \leqslant \frac{1}{1 + e^\alpha} \leqslant 1, \text{ for all } \alpha \in \mathcal{I}. \tag{63}$$

we conclude that $u^\top_{\mathrm{N},k+\theta} p_{\mathrm{N},k+1} \leqslant 0$. For the frictional term, $u^{\alpha,\top}_{\mathrm{T},k+\theta} p^\alpha_{\mathrm{T},k+1}$, we get

$$u^{\alpha,\top}_{\mathrm{T},k+\theta} p^\alpha_{\mathrm{T},k+1} = \theta u^{\alpha,\top}_{\mathrm{T},k+1} p^\alpha_{\mathrm{T},k+1} + (1-\theta) u^{\alpha,\top}_{\mathrm{T},k} p^\alpha_{\mathrm{T},k+1}. \tag{64}$$

The first term is non-positive but we cannot draw any conclusions about the sign of the second term. We will demonstrate that on a simple example this term can be positive and that the scheme will generate energy.

This fact is not particularly surprising. If we accept that the scheme is consistent and converges towards the continuous-time model, then we must converge towards a model that can generate energy. In practice, energy can be generated even in the case where we have reduced the time steps to obtain a more accurate solution.

Remark 2 *A possible way to dissipate energy it to cancel the second term in* (64) *using* $\theta = 1$. *In this case, the condition* (63) *will imply that* $e^\alpha = 0$ *for all* α. *This result coincides with the result obtained by Glocker (2013), who demonstrated that* $e = 0$ *is the only value of the restitution coefficient that can maintain energetic consistency in the case of unilateral kinematic and geometric constraints with coupling between the impact elements (as is the case when Coulomb friction is added to the system).*

3.2 Principles of the proposed scheme

The following proposal for a new time-stepping scheme differs in the way the contact law is discretised to obtain contact dissipation that is always positive. The Moreau–Jean based scheme with the Frémond impact law is defined as follows:

$$\begin{cases} M(v_{k+1} - v_k) + hKq_{k+\theta} + hCv_{k+\theta} - hF_{k+\theta} = H^\top(q_k) p_{k+1}, & \text{(65a)} \\ q_{k+1} = q_k + h v_{k+\theta}, u_{k+1} = H(q_k)\, v_{k+1}, & \text{(65b)} \\ -\Theta(u_{k+\theta}) \in \mathrm{N}_{\mathcal{K}}(p_{k+1}) & \text{(65c)} \end{cases}$$

with the function Θ as

$$\Theta^\alpha(u^\alpha) = u^\alpha + \begin{pmatrix} \left(\theta\left(1 + e^\alpha\right) - 1\right) u^\alpha_{\mathrm{N},k} + \mu^\alpha \|u^\alpha_{\mathrm{T}}\| \\ 0 \\ 0 \end{pmatrix}. \tag{66}$$

Let us enumerate what is solved in each of the three possible cases of the contact law:

1. The take-off case: $p^\alpha_{k+1} = 0$. In this case, we have

$$u^\alpha_{\mathrm{N},k+\theta} + \left(\theta\,(1+e^\alpha) - 1\right) u^\alpha_{\mathrm{N},k} + \mu^\alpha \|u^\alpha_{\mathrm{T},k+\theta}\| \geqslant \mu^\alpha \|u^\alpha_{\mathrm{T},k+\theta}\|, \tag{67}$$

which simplifies to

$$u^\alpha_{\mathrm{N},k+1} + e^\alpha u^\alpha_{\mathrm{N},k} \geqslant 0. \tag{68}$$

2. The sticking case: $\Theta^\alpha(u^\alpha_{k+\theta}) = 0$. In this case, we have $u^\alpha_{\mathrm{T},k+\theta} = 0$ and

$$u^\alpha_{\mathrm{N},k+\theta} + \left(\theta\,(1+e^\alpha) - 1\right) u^\alpha_{\mathrm{N},k} = 0, \tag{69}$$

which simplifies to

$$u^\alpha_{\mathrm{N},k+1} = -e^\alpha u^\alpha_{\mathrm{N},k}. \tag{70}$$

3. The sliding case: $p^\alpha_{k+\theta} \neq 0$ and $\Theta^\alpha(u^\alpha_{k+\theta}) \neq 0$. Then we have $p^\alpha_{k+\theta} \in \partial\mathcal{K}^\alpha$ and $\Theta^\alpha(u^\alpha_{k+\theta}) \in \partial\mathcal{K}^{\alpha,\star}$. This implies

$$u^\alpha_{\mathrm{N},k+\theta} + \left(\theta\,(1+e^\alpha) - 1\right) u^\alpha_{\mathrm{N},k} + \mu^\alpha \|u^\alpha_{\mathrm{T},k+\theta}\| = \mu^\alpha \|u^\alpha_{\mathrm{T},k+\theta}\|, \tag{71}$$

which simplifies to

$$u^\alpha_{\mathrm{N},k+\theta} + \left(\theta\,(1+e^\alpha) - 1\right) u^\alpha_{\mathrm{N},k} = 0, \tag{72}$$

and then

$$u^\alpha_{\mathrm{N},k+1} = -e^\alpha u^\alpha_{\mathrm{N},k}. \tag{73}$$

For the frictional part, we have

$$\|p^\alpha_{\mathrm{T},k+1}\| = \mu p^\alpha_{\mathrm{N},k+1} \text{ and } \|u^\alpha_{\mathrm{T},k+\theta}\| p^\alpha_{\mathrm{T},k+1} = -\|p^\alpha_{\mathrm{T},k+1}\| u^\alpha_{\mathrm{T},k+\theta}. \tag{74}$$

To summarise, the Newton impact law is defined in the same way as in the Moreau–Jean time-stepping scheme. For the normal part of the law, the pre-impact velocity is the velocity at the beginning of the time-step $u^\alpha_{\mathrm{N},k}$ and the post-impact velocity is the velocity at the end of the time step $u^\alpha_{\mathrm{N},k+1}$. However, in the new Moreau–Jean scheme with Frémond impact law time-stepping scheme the Coulomb friction law is written with the average velocity $u^\alpha_{\mathrm{T},k+\theta}$, rather than the velocity at the end of the time-step $u^\alpha_{\mathrm{T},k+1}$, as is the case in the classical Moreau–Jean scheme.

When $\theta = 1/2$, the function Θ^α simplifies to

$$\Theta^\alpha(u^\alpha) = \begin{pmatrix} u^\alpha_{\mathrm{N}} + \dfrac{1}{2}(e^\alpha - 1)u^\alpha_{\mathrm{N},k} + \mu^\alpha \|u^\alpha_{\mathrm{T}}\| \\ u^\alpha_{\mathrm{T}}. \end{pmatrix} \tag{75}$$

and the discrete contact law is

$$-\Theta\left(\frac{1}{2}\left[u_{k+1} + u_k\right]\right) \in \mathrm{N}_{\mathcal{K}}(p_{k+1}) \tag{76}$$

We can observe that the expression (75) is very similar to the expression of the function Ξ in (46). In practice, if the scheme converges, we can expect to approximate the Frémond impact law. When $\theta = 1$, the function Θ^α is

$$\Theta^\alpha(u^\alpha) = \begin{pmatrix} u^\alpha_{\mathrm{N}} + e^\alpha u^\alpha_{\mathrm{N},k} + \mu^\alpha \|u^\alpha_{\mathrm{T}}\| \\ u^\alpha_{\mathrm{T}} \end{pmatrix} = \Gamma(u^\alpha), \tag{77}$$

and the discrete contact law is

$$-\Theta(u_{k+1}) = -\Gamma(u_{k+1}) \in \mathrm{N}_{\mathcal{K}}(p_{k+1}). \tag{78}$$

We observe that the scheme is identical to the Moreau–Jean time-stepping scheme for the case of $\theta = 1$.

3.3 Discrete dissipation properties and energy balance

Let us now give a result concerning the dissipation of this new Moreau–Jean scheme with the Frémond impact law.

Proposition 1 *The new Moreau–Jean scheme with the Frémond impact law dissipates energy in the sense that*

$$\mathcal{E}(t_{k+1}) - \mathcal{E}(t_k) \leqslant W^{\mathsf{ext}}_{k+1} + W^{\mathsf{damping}}_{k+1}, \tag{79}$$

if

$$\frac{1}{2} \leqslant \theta \leqslant \frac{1}{1+\bar{e}} \leqslant 1. \tag{80}$$

where $\bar{e} = \max e^\alpha, \alpha \in \mathcal{I}$.

In other words, providing that (80) is satisfied, the variation of the total mechanical energy of the system is always less than or equal to the energy supplied by the external and damping forces.

Proof The discrete-time dissipation equality of the new Moreau–Jean scheme (65) over a time-step $[t_k, t_{k+1}]$ is also given by (58). Hence, we have

$$\left(\frac{1}{2} - \theta\right) \left[\|v_{k+1} - v_k\|_M^2 + \|q_{k+1} - q_k\|_K^2\right] \leqslant 0, \text{ if and only if } \theta \geqslant \frac{1}{2}. \tag{81}$$

All that remains to prove is that $u_{k+\theta}^\top p_{k+1} \leqslant 0$. Let us examine the three possible cases for a contact α:

1. The take-off case: $p_{k+1}^\alpha = 0$. In that case, we have $u_{k+\theta}^{\alpha,\top} p_{k+1}^\alpha = 0$.
2. The sticking case: $\Theta^\alpha(u_{k+\theta}^\alpha) = 0$. In that case, we have $u_{\mathrm{T},k+\theta}^\alpha = 0$ and then $u_{k+\theta}^{\alpha,\top} p_{k+1}^\alpha = u_{\mathrm{N},k+\theta}^\alpha p_{\mathrm{N},k+1}^\alpha$. From (69), we conclude that $u_{\mathrm{N},k+\theta}^\alpha \leqslant 0$ since $\theta \leqslant \dfrac{1}{1+\bar{e}}$ and $u_{\mathrm{N},k}^\alpha \leqslant 0$ and then $u_{k+\theta}^{\alpha,\top} p_{k+1}^\alpha \leqslant 0$ since $p_{\mathrm{N},k+1}^\alpha \geqslant 0$.
3. The sliding case: $p_{k+\theta}^\alpha \neq 0$ and $\Theta^\alpha(u_{k+\theta}^\alpha) \neq 0$. Then we have $p_{k+\theta}^\alpha \in \partial\mathcal{K}^\alpha$ and $\Theta^\alpha(u_{k+\theta}^\alpha) \in \partial\mathcal{K}^{\alpha,\star}$. From (72), we conclude that $u_{\mathrm{N},k+\theta}^\alpha \leqslant 0$ since $\theta \leqslant \dfrac{1}{1+\bar{e}}$ and $u_{\mathrm{N},k}^\alpha \leqslant 0$, and then $u_{\mathrm{N},k+\theta}^\alpha p_{\mathrm{N},k+1}^\alpha \leqslant 0$. For the frictional part, we have from (74):
$$u_{\mathrm{T},k+\theta}^{\alpha,\top} p_{\mathrm{T},k+1}^\alpha = -\mu^\alpha p_{\mathrm{N},k+1}^\alpha \|u_{\mathrm{T},k+\theta}^\alpha\| \leqslant 0. \tag{82}$$

□

Given that we demonstrated that the Frémond impact law is dissipative in continuous time for any physically meaningful values of e and μ, it is once again no surprise that an approximation of this law using a Moreau–Jean scheme is also dissipative when $\theta \geqslant \dfrac{1}{2}$. From a practical perspective, we are thus able to conduct numerical integrations of complex systems with multiple impacts and friction (such as arise in simulating granular media or finite-element-discretised bodies undergoing contact) with guarantees on the stability of the solver, increasing both the speed and accuracy of the resolution.

4 Implementation details in Siconos

We will give some details of the implementation of the numerical solver as it is implemented in Siconos (Acary et al., 2019), where it is possible to solve the systems (54) and (65) directly. If the inverse of the mass matrix is simple (*i.e.* it is a diagonal or block diagonal matrix), we can also decide to reduce the system to the contact variable, as we do in the following. We will ultimately arrive at a second order cone complementarity problem for each scheme. Siconos/numerics implements a variety of solvers for second order cone complementarity problems, specifically for those arising in non-associative plasticity or friction problems (see for instance Acary et al., 2018) defined by the system

$$\begin{cases} w = Ar + b, \\ \tilde{w} = \Phi(w), \\ -\tilde{w} \in \mathrm{N}_{\mathcal{K}}(r), \end{cases} \tag{83}$$

where w and r are the vectors that solve the system, A is a matrix, b is a vector and Φ is an function that transforms w to the vector $\tilde{w}$ that has the complementarity relationship with r. In the following, Φ is the De Saxcé velocity function. Siconos has a built-in frictional contact problem type that automatically applies the De Saxcé function, which we exploit in our numerical solutions. Among the available solvers for this type of system, we may cite a) projection-based solvers for variational inequalities, b) iterative solvers such as block projected Gauss–Seidel, c) semi-smooth Newton methods, and d) interior point methods (Acary et al., 2023). The solver finds the values of r and w that resolve the system to a given tolerance, using the norm $\dfrac{\|r - \mathrm{proj}_{\mathcal{K}}(r - \Phi(Ar+b))\|_2}{1 + \|b\|_2}$, which we set to 10^{-10} (unless otherwise specified), *i.e.* we resolve our systems with very small error. We will exploit the nonsmooth Gauss–Seidel solver (Jourdan et al., 1998) to resolve our systems, as it is a very robust solver.

4.1 Implementation of the Moreau–Jean scheme

To arrive at the appropriate cone complementarity system for the classical Moreau–Jean scheme, we expand the first line of (65a) to obtain

$$\left(M + h\theta C + h^2\theta^2 K\right) v_{k+1} = \left(M - h(1-\theta)C - h^2\theta(1-\theta)K\right) v_k - hKq_k + hF_{k+\theta} + H^\top(q_k) p_{k+1}. \tag{84}$$

Then, we construct the matrix $\hat{M} = M + h\theta C + h^2\theta^2 K$ and obtain an expression for the relative velocities given by

$$u_{k+1} = H(q_k)\hat{M}^{-1}\left[\left(M - h(1-\theta)C - h^2\theta(1-\theta)K\right) v_k - hKq_k + hF_{k+\theta}\right] + H(q_k)\hat{M}^{-1}H^\top(q_k) p_{k+1}. \tag{85}$$

We will denote the discrete Delassus matrix W by

$$W = H(q_k)\hat{M}^{-1}H^\top(q_k), \tag{86}$$

and a constant term by

$$y = H(q_k)\hat{M}^{-1}\left[\left(M - h(1-\theta)C - h^2\theta(1-\theta)K\right)v_k - hKq_k + hF_{k+\theta}\right]. \tag{87}$$

We obtain a second order cone complementarity problem that must be solved at each time step:

$$\begin{cases} u_{k+1} = Wp_{k+1} + y, \\ -\Gamma(u_{k+1}) \in \mathrm{N}_{\mathcal{K}}(p_{k+1}). \end{cases} \tag{88}$$

Now, considering the generic system (83), we set $A = W$, $b^\alpha = y^\alpha + \begin{bmatrix} eu^\alpha_{\mathrm{N},k} \\ 0 \\ 0 \end{bmatrix}$, r is the vector of percussions over the time step p_{k+1} and w the vector of De Saxcé relative velocities at the end of the time step u_{k+1}, respectively. r and w will be resolved by the solver so that they fulfil the system (88).

4.2 Implementation of the new Moreau–Jean scheme

For the new scheme, we expand the first line of (65) to obtain the same expression as (84). Then, adding $\left(M + h\theta C + h^2\theta^2 K\right)v_k$ to each side and making the appropriate rearrangements and simplifications leads to

$$(M + h\theta C + h^2\theta^2 K)v_{k+\theta} = Mv_k - h\theta Kq_k + h\theta F_{k+\theta} + \theta H^\top(q_k)p_{k+1}. \tag{89}$$

Once again constructing the matrix $\hat{M} = M + h\theta C + h^2\theta^2 K$, inverting it and multiplying by $H(q_k)$, we obtain an expression for the relative velocities:

$$u_{k+\theta} = H(q_k)\hat{M}^{-1}(Mv_k - h\theta Kq_k + h\theta F_{k+\theta}) + \theta H(q_k)\hat{M}^{-1}H^\top(q_k)p_{k+1}. \tag{90}$$

By denoting the discrete Delassus matrix

$$W = \theta H(q_k)\hat{M}^{-1}H^\top(q_k), \tag{91}$$

and the constant term

$$y = H(q_k)\hat{M}^{-1}(Mv_k - h\theta Kq_k + h\theta F_{k+\theta}), \tag{92}$$

the following second order cone complementarity problem

$$\begin{cases} u_{k+\theta} = Wp_{k+1} + y, \\ -\Theta(u_{k+\theta}) \in \mathrm{N}_{\mathcal{K}}(p_{k+1}), \end{cases} \tag{93}$$

has to be solved at each time step. We set $A = W$, $b^\alpha = y^\alpha + \begin{bmatrix} (\theta(1+e^\alpha)-1)u^\alpha_{\mathrm{N},k} \\ 0 \\ 0 \end{bmatrix}$, and find the vectors r and w (respectively the vectors of percussions over the time step p_{k+1} and the mid-step local relative velocities $u_{k+\theta}$) that provide us with a solution of (93).

5 Numerical illustrations

Here, we demonstrate on several different example systems the difference between the results obtained using the classical Moreau–Jean scheme with discrete Moreau's impact law and Coulomb's friction, against those obtained using the new proposed scheme with discrete Moreau's impact law and Coulomb's friction, for systems described in continuous time by equation (31).

5.1 Impacting stick

The first example is a rigid bar impacting a fixed, rigid obstacle. This very simple example shows the errors in calculating dissipation in discrete time using the classical Moreau–Jean scheme. We consider a bar of length l and mass m subjected to gravity. Its centre of mass G is given by the coordinates (x, y) and the angle of the bar γ complete the generalised coordinates (see Figure 1). For simplicity's sake, the contact point C is considered to be on the middle fibre of the bar. The numerical values (in dimensionless units) are as follows: $m = 1, l = 1, g = 10, e = 1.0, \mu = 0.01$ and the initial conditions are $q_0 = \left(\frac{1}{2}l\sin(\pi/4), \frac{1}{2}l\cos(\pi/4) + 0.01, \pi/4\right)$ and $v_0 = (-0.5, 0.1, 0.1)$.

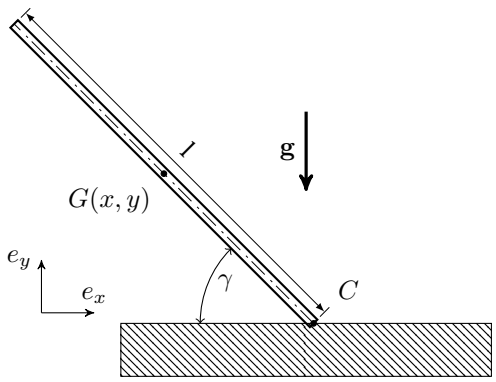

Figure 1: The geometry of the impacting stick of length l with a centroid at G and making contact with the ground at point C, at an angle of γ.

The simulation is performed with a time step $h = 10^{-4}$, $\theta = 0.5$ and a simulation interval $[0, 0.2]$ to observe the first two impacts in detail, using both the classical and new schemes. The results are displayed in Figure 2 and Figure 3.

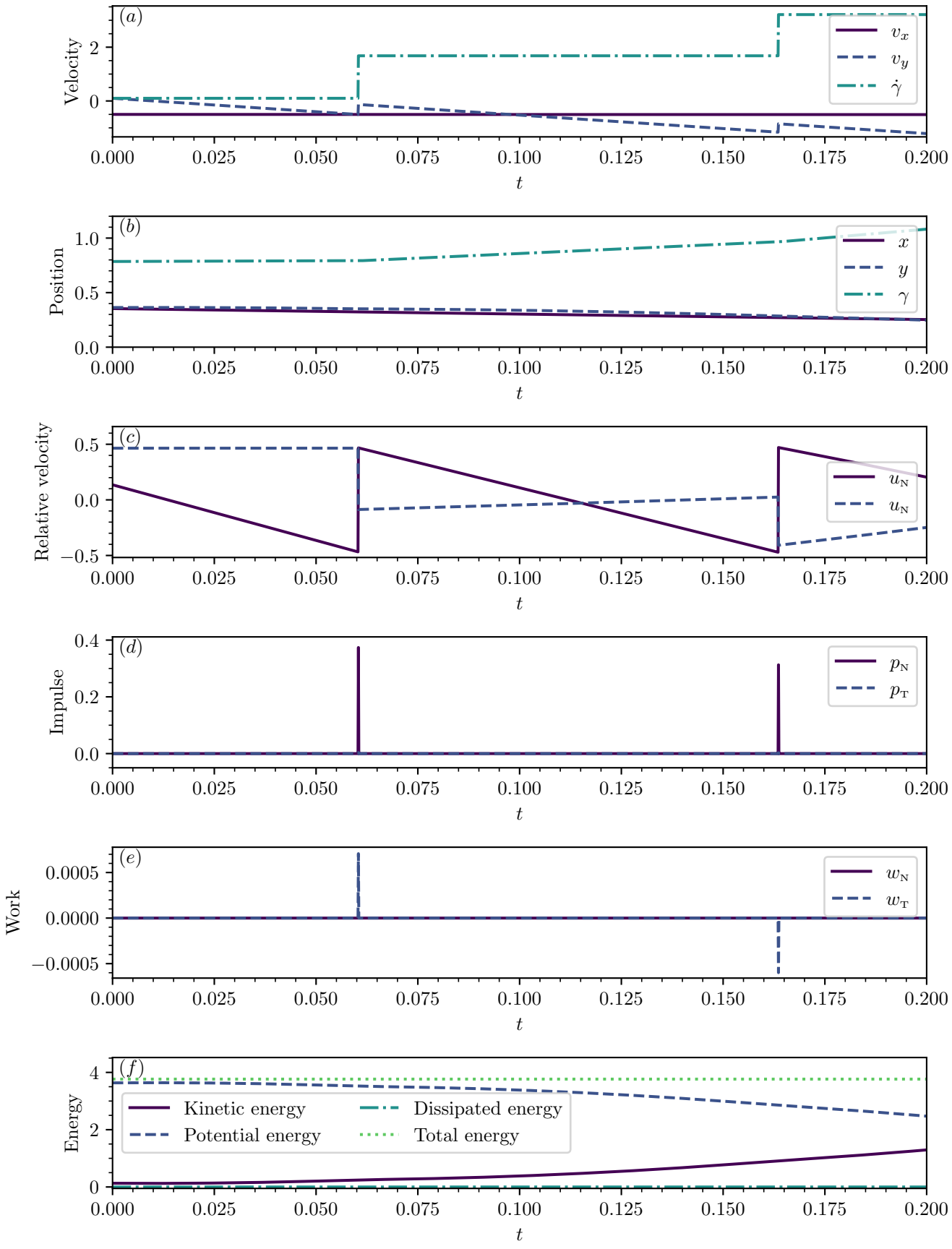

Figure 2: The results of the simulation of the impacting stick, using the standard Moreau–Jean scheme, with $\theta = 0.5, h = 10^{-4}$. (a) The generalised displacements of the system. (b) The global velocities of the system. (c) The local relative normal and tangential velocities. (d) The normal and tangential contact percussions. (e) The work done by the percussions and local velocities. (f) The total energetic quantities of the system.

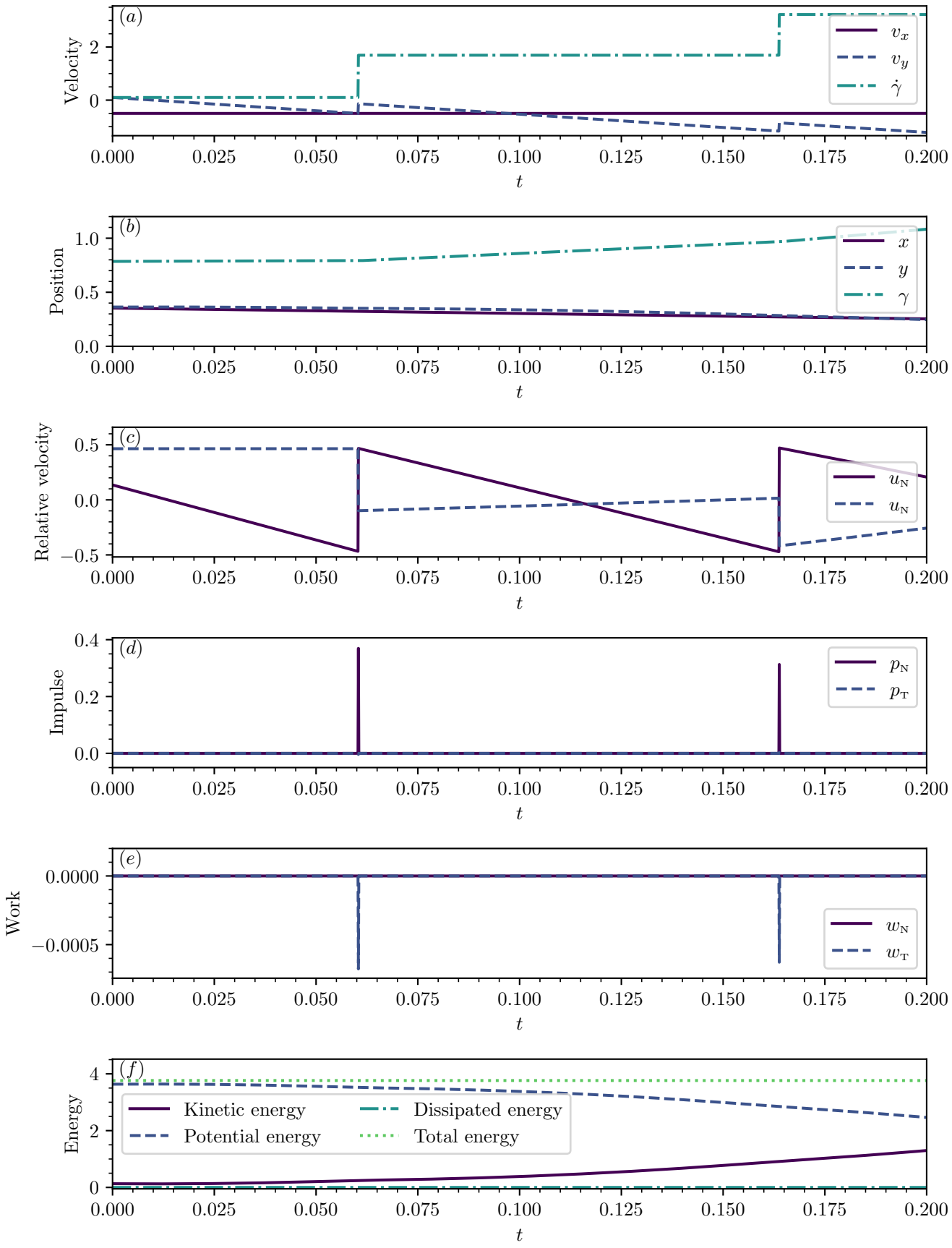

Figure 3: The results of the simulation of the impacting stick, using the new Moreau–Jean scheme with the Frémond law, with $\theta = 0.5, h = 10^{-4}$. (a) The generalised displacements of the system. (b) The global velocities of the system. (c) The local relative normal and tangential velocities. (d) The normal and tangential contact percussions. (e) The work done by the percussions and local velocities. (f) The total energetic quantities of the system.

It is observed that the energy dissipated by friction can have the wrong sign for the Moreau–Jean scheme with Newton law at first impact, and therefore generate energy, which is not the case for the proposed Moreau–Jean scheme with the Frémond law. We also observe here that while the normal percussions at impact occur, they do no net work on the system due to the choice of $e = 1$.

5.2 A rocking block

We now consider a rigid block of mass m, length b and height l, subjected to gravity. The centroid of the block is located at $G(x, y)$, and the generalised coordinates are completed by the angle to the horizontal plane γ. It is assumed that the block makes contact with the rigid ground at its two corner points C_1 and C_2. The geometry is depicted in Figure 4. The numerical values of the system (once again in dimensionless units) are $b = 1$, $l = 1$, $m = 1$, $g = 10$, $e = 1.0$, $\mu = 0.1$. The initial conditions are $q_0 = (0, 0.6, 0)$ and $v_0 = (0, -0.2, 1)$.

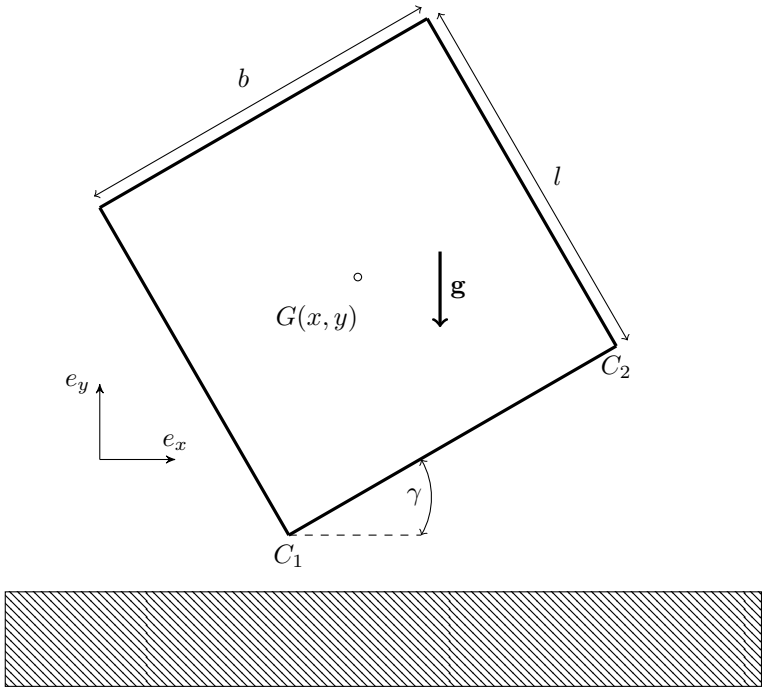

Figure 4: A rocking block of width b and height h, with a centroid at G and making contact with the ground at the points C_1 and C_2, at an angle of γ.

The simulation is performed with a time step $h = 10^{-4}$, $\theta = 0.5$ and a simulation interval $[0, 1]$, using both the classical and new schemes. The results are displayed in Figure 5 and Figure 6.

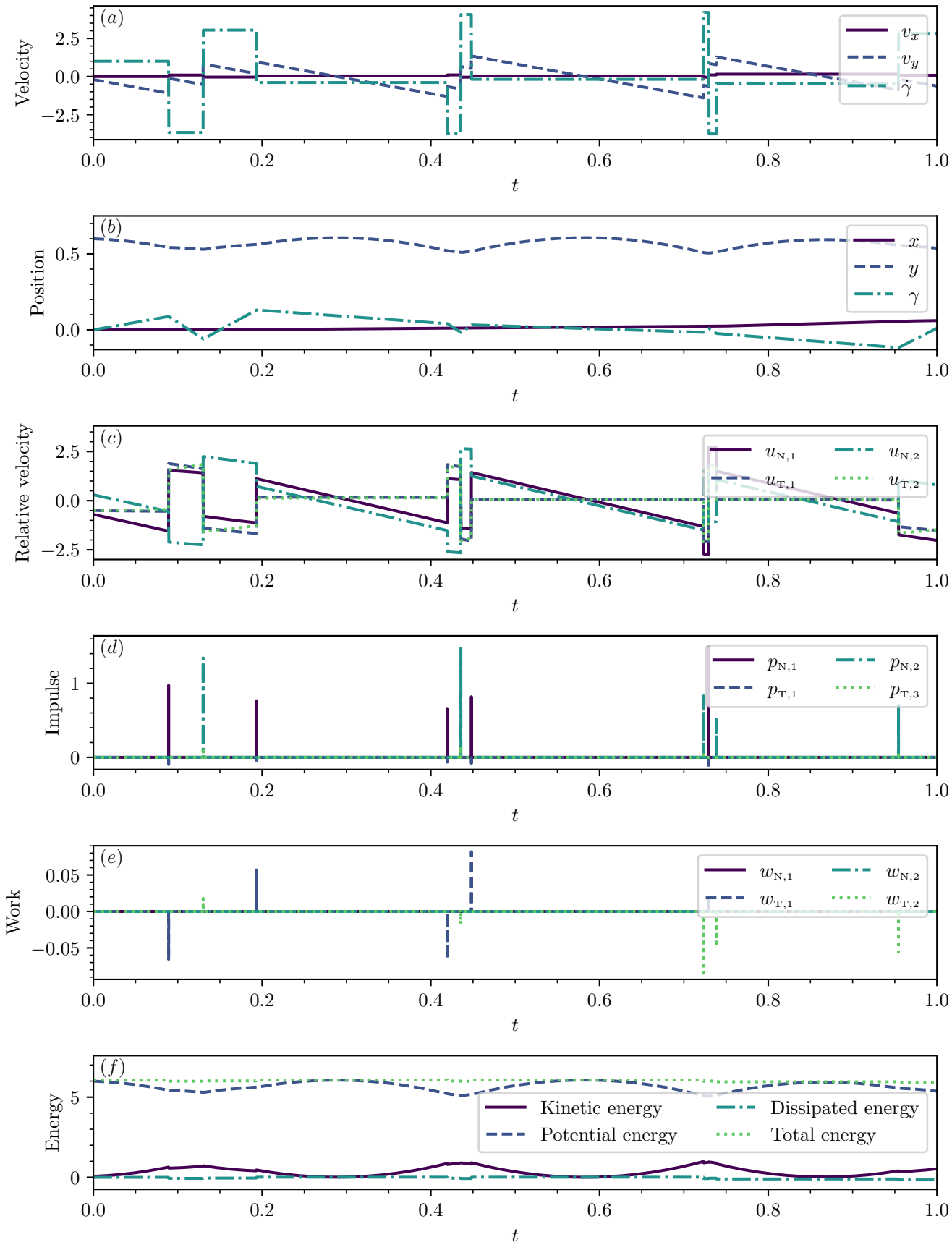

Figure 5: The results of the simulation of the rocking block, using the standard Moreau–Jean scheme, with $\theta = 0.5, h = 10^{-4}$. (a) The generalised displacements of the system. (b) The global velocities of the system. (c) The local relative normal and tangential velocities. (d) The normal and tangential contact percussions. (e) The work done by the percussions and local velocities. (f) The total energetic quantities of the system.

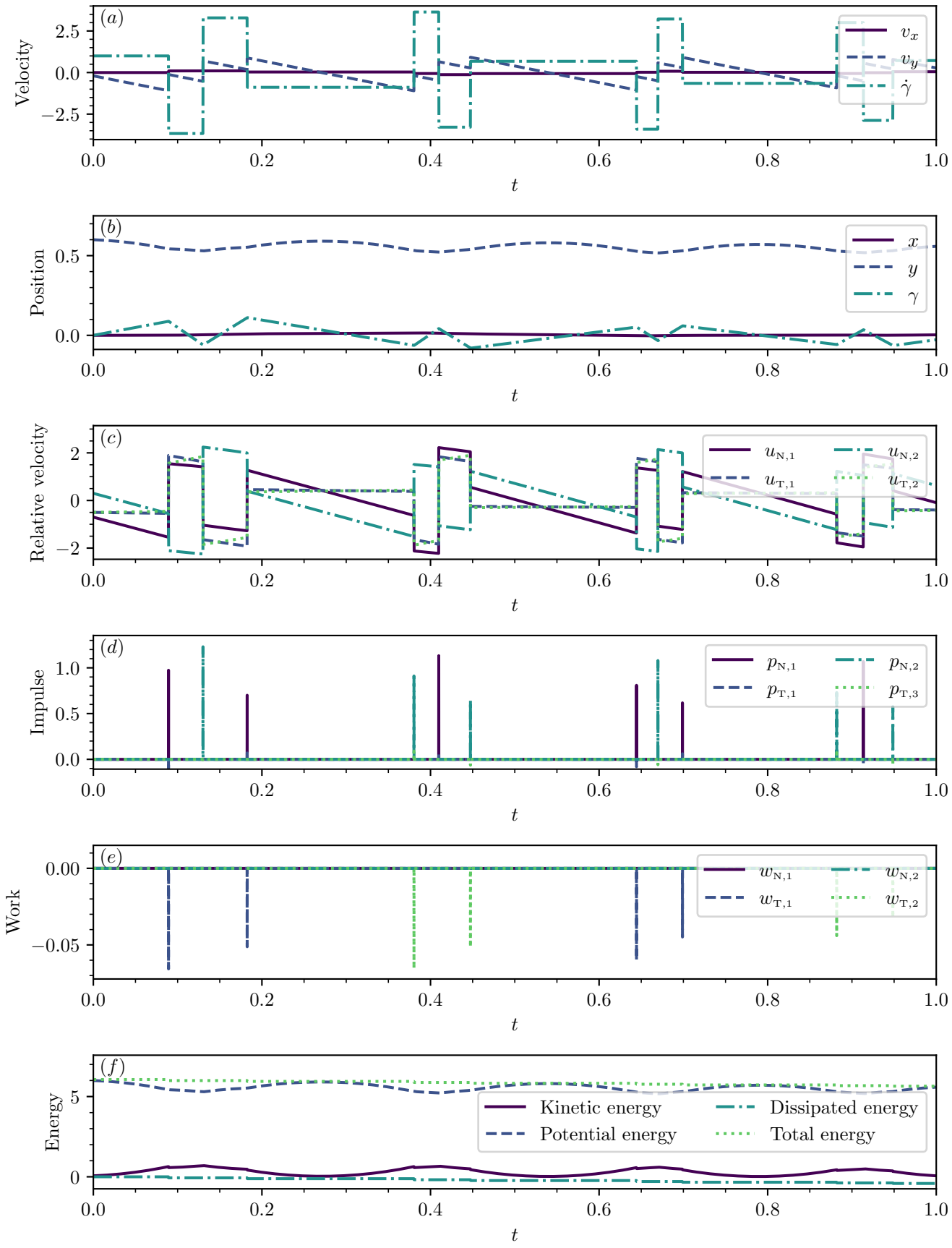

Figure 6: The results of the simulation of the rocking, using the new Moreau–Jean scheme with the Frémond law, with $\theta = 0.5, h = 10^{-4}$. (a) The generalised displacements of the system. (b) The global velocities of the system. (c) The local relative normal and tangential velocities. (d) The normal and tangential contact percussions. (e) The work done by the percussions and local velocities. (f) The total energetic quantities of the system.

As can be clearly seen, the classical Moreau–Jean scheme with the Newton law creates energy at the second, third, sixth and eighth impacts, and in fact the dissipated energy can be become positive. The global effect of this can be seen in the total energy curve in Figure 5(f) where the total energy has visible "kinks" as a sequence of impacts first dissipates then creates energy. By comparison, Figure 6 demonstrates clearly the difference with the system being purely dissipative, and each impact either doing no dissipative work (as $e = 1$, so the normal part of the impact is purely elastic), or doing negative work due to frictional sliding. The total energy curve clearly decreases at each impact, as would be expected. A comparison of the velocities and positions of the system's centre of mass presented in the subfigures (a) and (b) of each figure demonstrate plainly that the creation of energy in the Moreau–Jean scheme with Newton law has substantial effects on the system trajectory.

5.3 A sliding block

In this example we consider a linear elastic block that slides in constant contact with a rigid surface, with the geometry as shown in Figure 7.

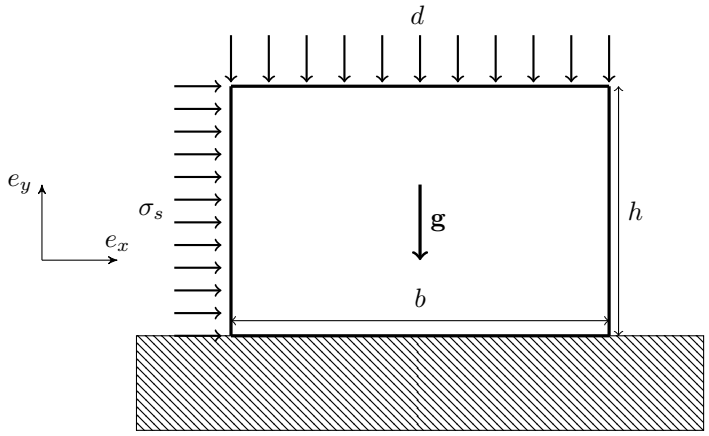

Figure 7: A sliding block under self-weight due to a gravity and an applied sliding force F_s. The height h is 25 mm and the breadth b is 40 mm. The thickness is set to 15 mm.

The block is taken to be made of Poly(methyl methacrylate) (PMMA), and to be linearly elastic. We take the linear elasticity parameters from Berman et al. (2020). We thus have the Young's modulus $E = 5.75 \times 10^3$ MPa, the Poisson's ratio $\nu = 0.358$ and the density $\rho = 1.17 \times 10^{-3}$ g/mm^3. We choose a value of the restitution coefficient e of 0.0 and friction coefficient $\mu = 0.5$, and apply these values to all contact nodes.

We discretise the system in space using the finite element method, generating the mesh with Gmsh 4.11.1 (Geuzaine and Remacle, 2009) and setting a characteristic length of 1 mm throughout, then reading it in to Python 3.12.1 with meshio 5.3.5 (Schlömer, 2022). We use linear triangle (T3) elements with a single Gauss point and a consistent mass matrix, choose the plane stress simplifying assumption, and work in the linear finite element framework (that is to say that the finite element matrices are calculated once with respect to the undeformed system configuration (shown in Figure 8(a)) and remain constant for the entire simulation).

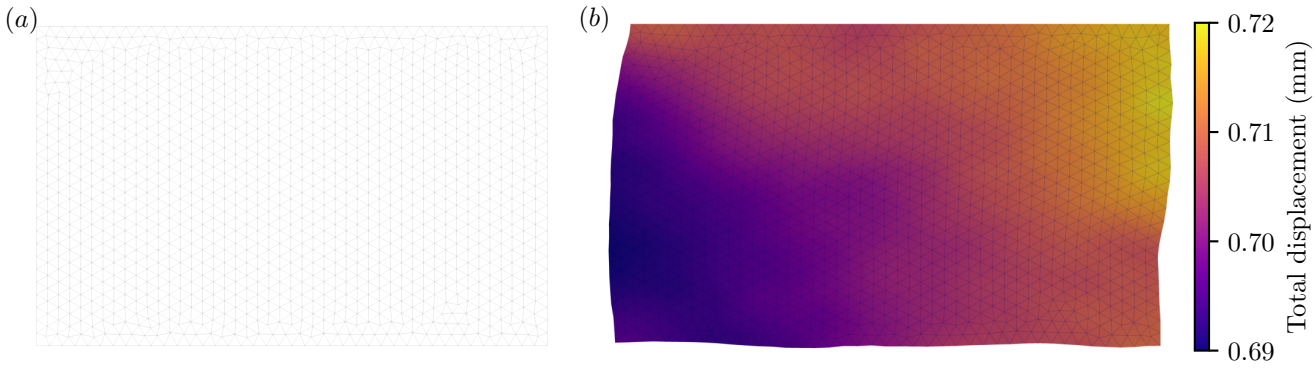

Figure 8: Mesh of the sliding block. (a) The block mesh in the undeformed configuration. (b) The block mesh in the deformed configuration at $t = 0.3$, using the Moreau–Jean scheme with Frémond law, with a $100\times$ warp factor applied to the mesh to exaggerate the displacements, which are also shown via the colour bar. Both figures are generated by ParaView (Ahrens et al., 2005).

The system is first subjected to an applied vertical displacement $d = -0.005$ mm along the top boundary and the initial displacements are resolved elastically with the no slip and no interpenetration conditions enforced at the contact boundary. During the simulation, the block is subjected to its own self-weight (with gravity set to be -10^{-3} mm/ms^2), the vertical displacement on the top boundary is held constant and an oscillating traction σ_s on the left boundary given by

$$\sigma_s = 2\,\mathrm{sgn}\left[\sin\left(4\pi t\right)\right]. \tag{94}$$

We simulate the system for 1 ms, with time steps of 10^{-4} ms, so as to ensure a very fine resolution of the system.

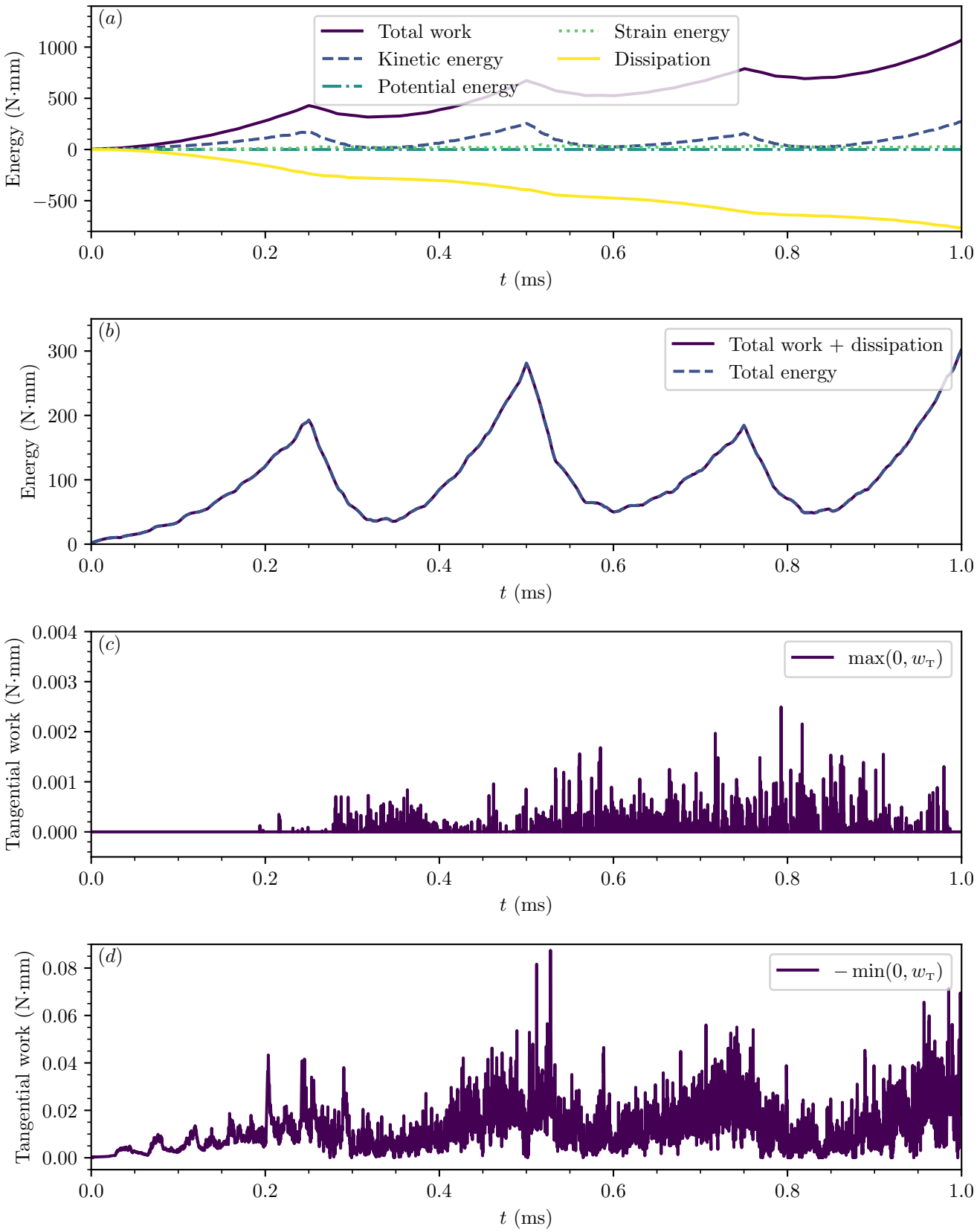

Figure 9: The results of the simulation using the classical Moreau–Jean method with $\theta = 0.5$ and $h = 10^{-4}$ ms. (a) The individual energetic components of the simulation. (b) The sum of the work input to the system with the dissipation, compared to the total energy of the system. (c) The maximum value of the positive part of the tangential work w_{T} over all contact nodes at each time step. (d) The minimum value of the negative part of the tangential work w_{T} over all contact nodes at each time step.

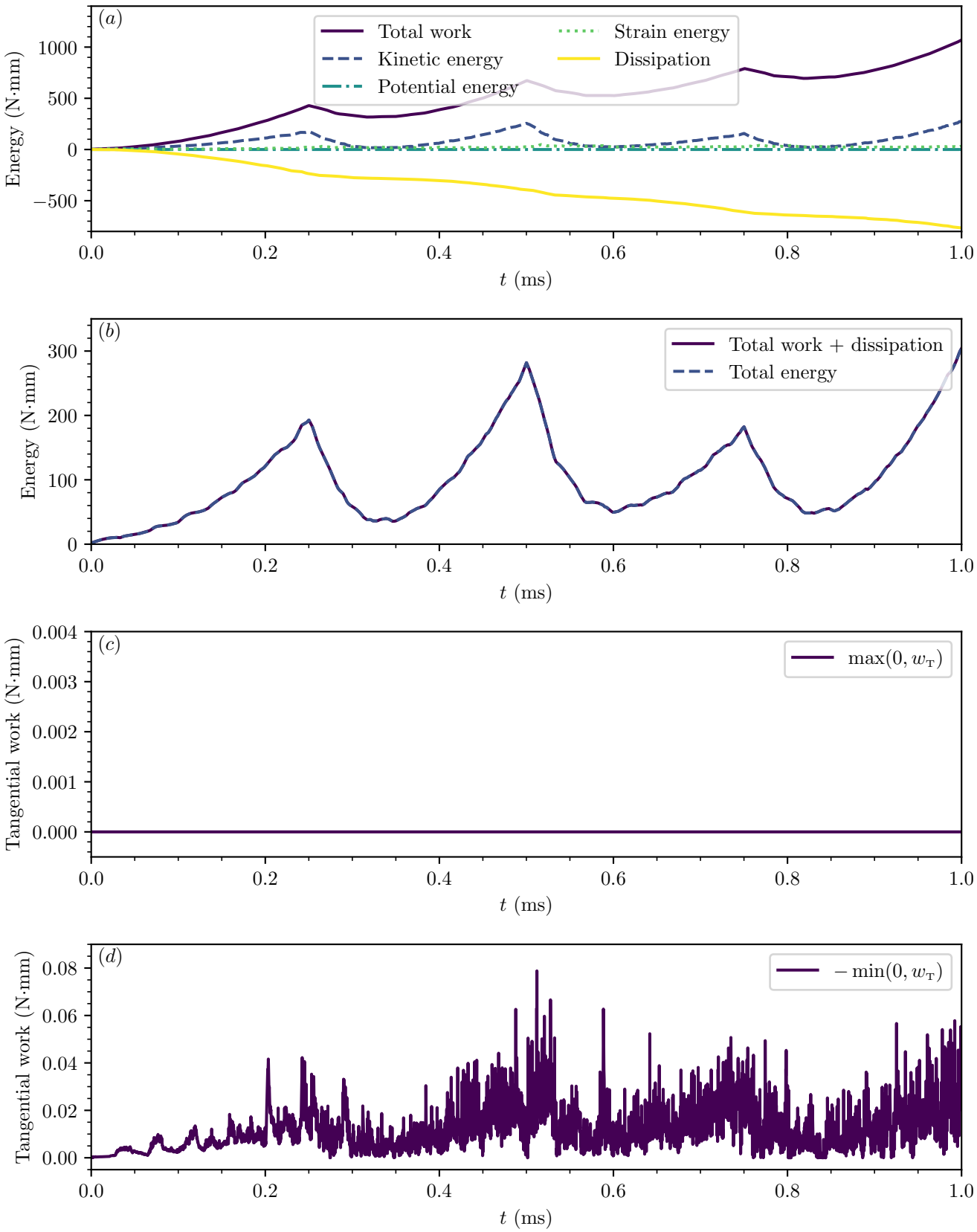

Figure 10: The results of the simulation using the new Moreau–Jean method with the Frémond law and with $\theta = 0.5$ and $h = 10^{-4}$ ms. (a) The individual energetic components of the simulation. (b) The sum of the work input to the system with the dissipation, compared to the total energy of the system. c) The maximum value of the positive part of the tangential work w_{T} over all contact nodes at each time step. (d) The minimum value of the negative part of the tangential work w_{T} over all contact nodes at each time step.

When comparing Figure 9 and Figure 10, we can see very clearly that the new scheme completely avoids generating positive tangential work, aligning with the analytical proofs above. In this case, the rest of the system is dissipative enough to overcome the energy created by the Moreau–Jean scheme, meaning that the global system remains stable and the sum of the total work and dissipation tracks the total energy closely in both cases.

It is also worth remarking on the seeming appearance of Schallamach-type waves (Schallamach, 1971) (namely true Schallamach waves, separation pulses and slip pulses) along the bottom surface of the block, visible in Figure 8(b). Previous studies (Barquins, 1985; Viswanathan and Chandrasekar, 2022) have emphasised the role played by adhesion, viscoelastic and temperature effects in this phenomenon. While we have not included it in the simulations in this paper, our method includes the possibility of linear viscosity in the damping matrix C, and setting $e = 0$ (a perfectly inelastic contact), as we have in these simulations, we can at least treat the limiting case of zero adhesive force. Further, experimental evidence suggests that propagating frictional ruptures have a complex spatial structure (Berman et al., 2020), suggesting the importance of rate-dependent friction. As this article is dedicated to the description of a theoretical and numerical model, we will not explore this subject any further, beyond noting that having a consistently dissipative numerical method like the new scheme would seem to be a precondition to a robust numerical study of these phenomena, which have more typically been explored theoretically and experimentally.

5.4 Impact on masonry structure

In this example we consider a more practical example of a rockfall impacting on a masonry wall, with the geometry shown in Figure 11. The wall has 10 layers of blocks, and is buttressed by six buttresses, composed of the same type of blocks. The wall rests on flat ground, and in front of the wall is a slope at 45°. Each block has a width of 1 m, a depth of 2 m and a height of 1 m. A rock of approximately 5 m diameter is created with an irregular polyhedral shape, which then has its contour shrunk by 10% in order to improve its contact detection properties.

The blocks and the rock are taken to be rigid bodies, subject to gravity of 9.81m/s^2. All the bodies are taken to have a density of 2300 kg/m^3. The Newton coefficient of restitution for all normal impacts is taken as $e = 0.2$ and the coefficient of friction as $\mu = 0.6$.

To obtain accurate results, the simulation is run for 4 s, starting at $t = 0$, with time steps of $h = 5 \times 10^{-4}$ and $\theta = 0.5$. The rock is created at $t = 0.01$, its initial position is at the coordinates (30, 0, 35) m and it has an initial translational velocity of (-10, 0, -35) m/s and an angular velocity of (0.5, 10, 0.1) s^{-1}.

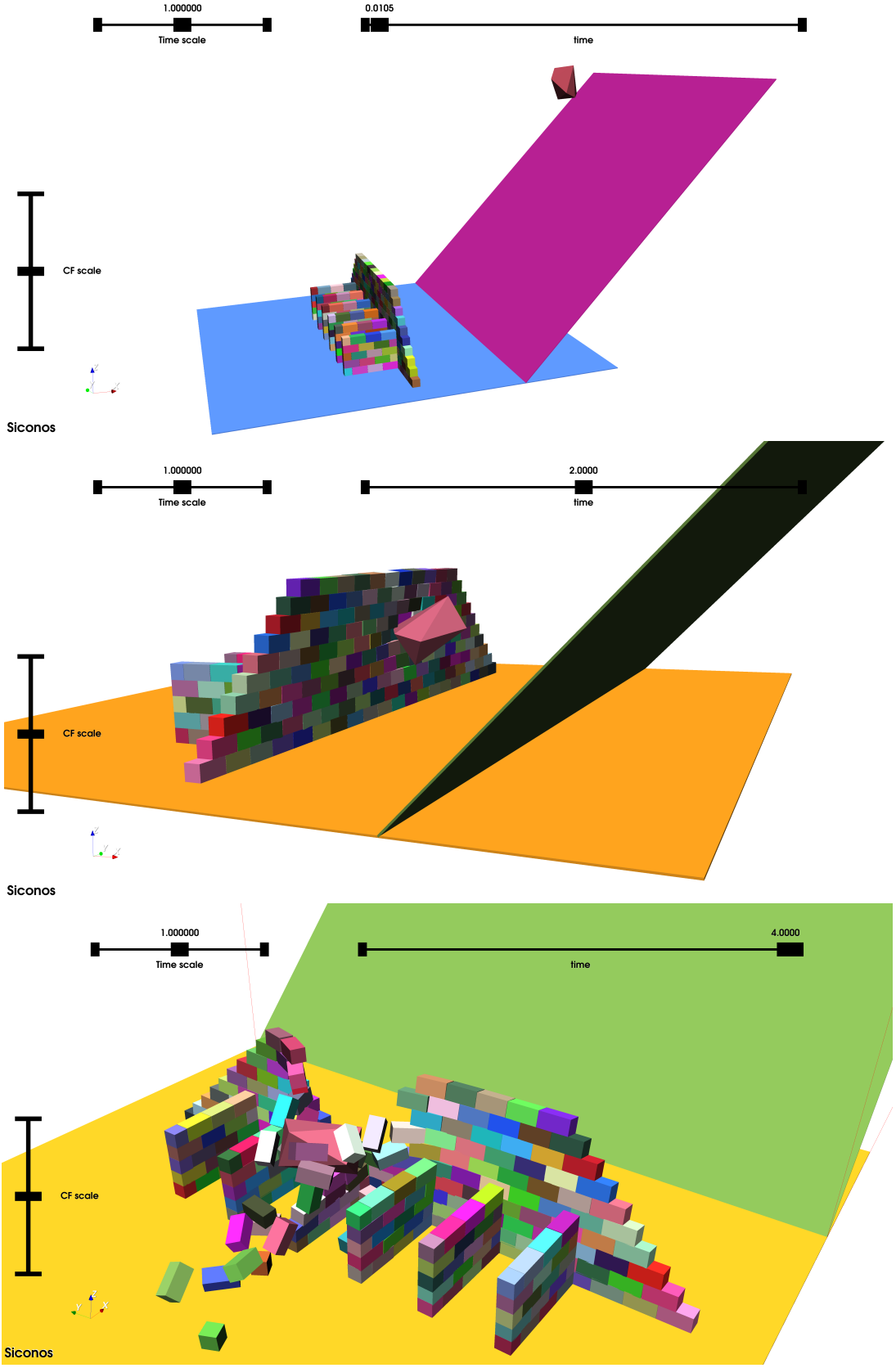

Figure 11: Impact of a rock on a masonry structure, at the point of creation of the rock, just after impact, and at the end of the simulation.

In the first instance, we highlight that we are pushing the system outside the range for which the proofs above are valid, *i.e.* rather than a linear Lagrangian system we have a Newton–Euler system. However, in practical terms, this does not prevent the model being implemented as a reasonable approximation. The particularly pertinent differences to note from the system described in (31) are that the generalised coordinate vector q contains information about the centre of mass of each block and the impacting rock, as well as its orientation with respect to a fixed inertial frame encoded as quaternions. As a consequence,

we can no longer say $\dot{q}(t) = v(t)$, but instead require a transformation depending on the generalised coordinate to be applied *i.e.* $\dot{q}(t) = T(q)v(t)$, where $T(q)$ is a matrix that acts to transform the time derivative of the quaternions into conventional angular components in the body-fixed frame. With this convention, the mass matrix remains constant. Secondly, we track the total work done by the external and gyroscopic forces of the system over each increment of time, given by

$$W_{k+1} = v_{k+\theta}^{\top}\left(F_{k+\theta}^{\mathsf{ext}} + F_{k+\theta}^{\mathsf{gyr}}\right) \approx \int_{t_k}^{t_{k+1}} \frac{1}{2}(v^{+}(t) + v^{-}(t))^{\top}\left(F^{\mathsf{ext}}(t) + F^{\mathsf{gyr}}(t)\right)\mathrm{d}t. \tag{95}$$

The system is resolved with Siconos' three dimensional nonsmooth Gauss–Seidel frictional solver, with the tolerance set to 10^{-4}, and the contact detection resolved with Siconos' internal version of Bullet (Coumans and Bai, 2016–2021). For a full list of the various numerical tolerances implemented in the system, we refer readers to the simulation file (Acary, 2024). The results of the simulation are output at every time step.

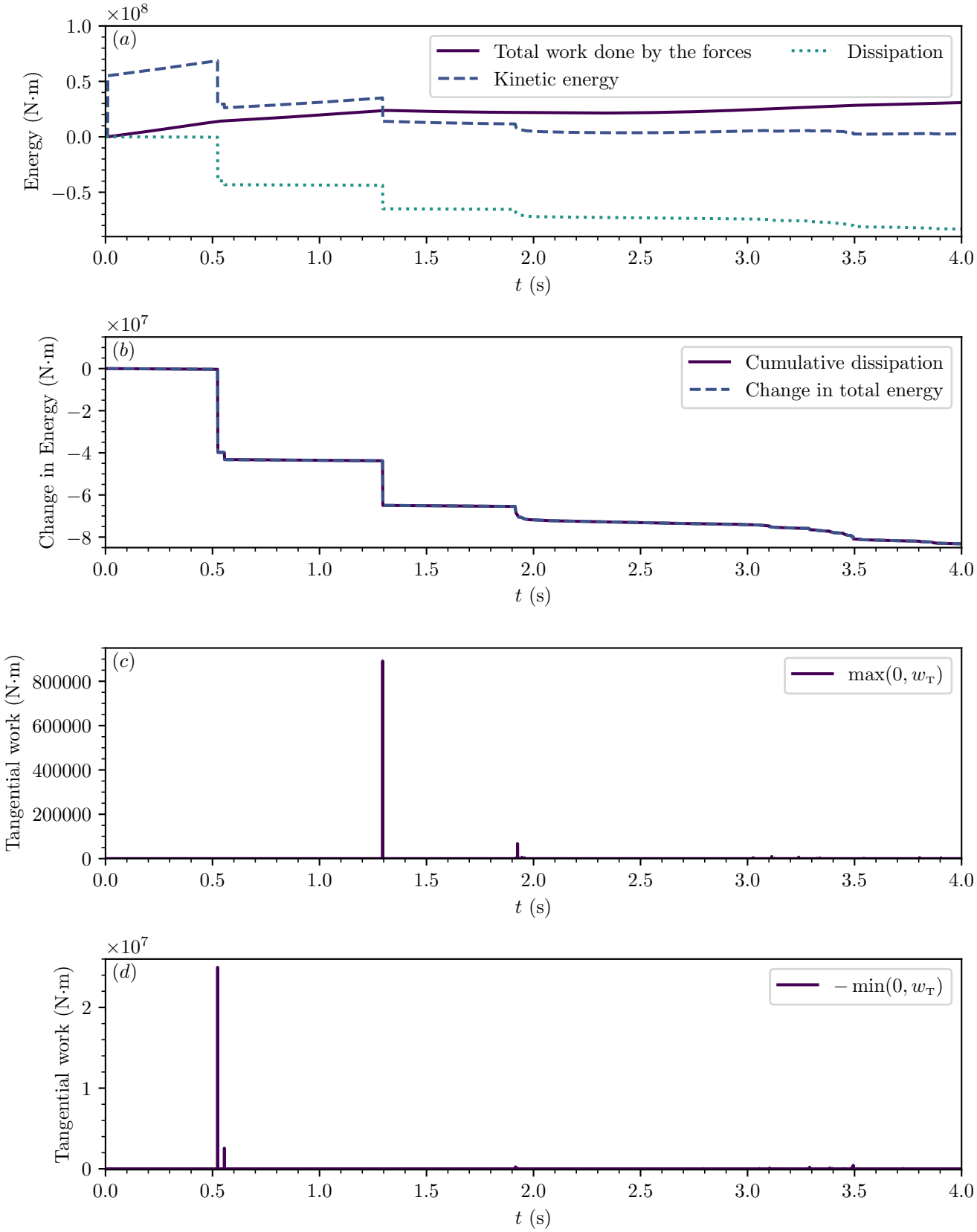

Figure 12: The results of the simulation using the classical Moreau–Jean method with $\theta = 0.5$ and $h = 0.0005$ s. (a) The individual energetic components of the simulation. (b) The sum of the change in energy work of the system with the cumulative dissipation. (c) The maximum value of the positive part of the tangential work w_{T} over all contact nodes at each time step. (d) The minimum value of the negative part of the tangential work w_{T} over all contact nodes at each time step.

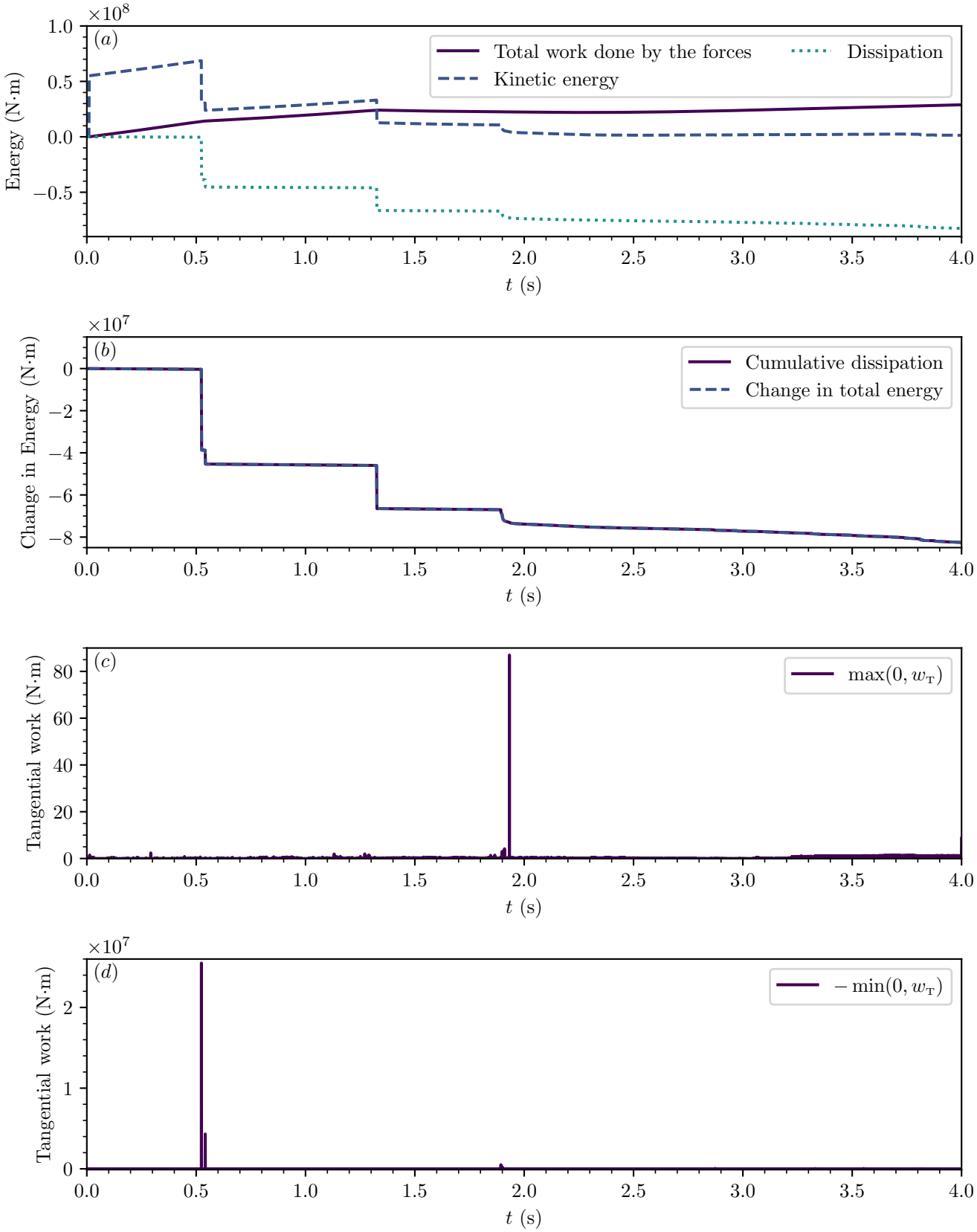

Figure 13: The results of the simulation using the proposed method $\theta = 0.5$ and $h = 0.0005$ s. (a) The individual energetic components of the simulation. (b) The sum of the change in energy work of the system with the cumulative dissipation. c) The maximum value of the positive part of the tangential work w_{T} over all contact nodes at each time step. (d) The minimum value of the negative part of the tangential work w_{T} over all contact nodes at each time step.

In contrast to the previous examples, we see that in this case, the proposed scheme does on occasion generate positive

tangential work. This is a direct consequence of numerical error related to the relatively large time step and solver tolerance chosen. With a tighter numerical tolerance, the positive part of the tangential work goes towards zero, and in any case the magnitude of the positive part remains three orders of magnitude less than that seen in the classical Moreau–Jean method. We can compare more closely the total dissipation of each method in Figure 14:

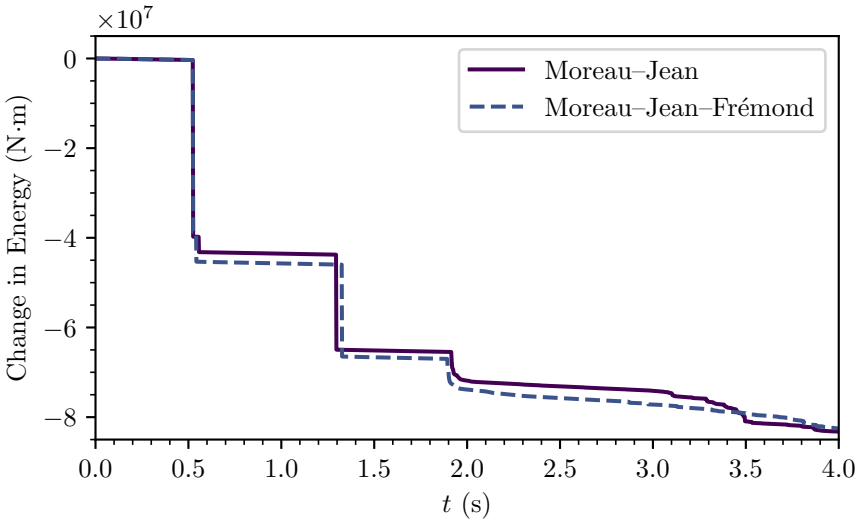

Figure 14: The total dissipation of the system for each method.

We can see that where we have clear corresponding impacts in the two systems, the proposed method clearly dissipates more energy, as a consequence of having smaller positive tangential work terms. As a result, the system has less kinetic energy, and so there are fewer impacts with noticeable dissipation than in the corresponding Moreau–Jean system. In particular, at about 3.1 seconds into the simulation, the increased energy in the Moreau–Jean system causes a number of impacts to occur without the new scheme having obviously corresponding impacts (however, the solution with the proposed scheme does have a small accumulation of impacts near the end without an obvious analogue in the Moreau–Jean scheme). Ultimately, the two systems end up having dissipated similar amounts of energy, although the difference in magnitude of each impacting event causes the systems to follow noticeably different paths to get there.

6 Conclusion

In this article, we have demonstrated that the Frémond model of frictional contact gives a treatment of Coulomb friction combined with Newton's impact law that is always dissipative in continuous time. By adapting the Moreau–Jean time integration scheme to approximate the Frémond model in discrete time, we are able to develop a numerical method that is also provably always dissipative. We then considered several examples and demonstrated that in cases where the classical Moreau–Jean scheme creates energy, the new scheme demonstrably does not. This work demonstrates new results and techniques that are likely to be of significance across a variety of subfields in mechanics, ranging from simulations of granular media to design of mechanical linkages. In future extensions of this work, we expect to generalise it to the case of nonlinear systems (Newton–Euler equations or nonlinear systems that derive from potentials), consider large sliding problems that are generally best treated with a mortar method (Puso et al., 2024), and to consider the possibility of other impact laws such as those including a cohesion acting on the surface (Collins-Craft et al., 2024).

Acknowledgements

The authors acknowledge the support of the European Research Council (ERC) under the European Union Horizon Europe research and innovation program (Grant agreement 101064805 LEMMA). We thank Franck Bourrier and Ritesh Gupta for their helpful comments on the manuscript.

Code and data availability

The code required to run the simulations described in this paper is available in a GitHub repository archived on Software Heritage, or alternatively on Zenodo. The sole exception to this is the code required to run the rockfall impact code, which is archived separately on Software Heritage as part of the Siconos tutorial repository. The data outputs of the codes are also available on Zenodo.

References

Brogliato, B. (2016). *Nonsmooth Mechanics: Models, Dynamics and Control*. 3nd. Communications and Control Engineering. London: Springer-Verlag.

Acary, V. (May 2016). "Energy conservation and dissipation properties of time-integration methods for nonsmooth elastodynamics with contact". In: *Journal of Applied Mathematics and Mechanics / Zeitschrift für Angewandte Mathematik und Mechanik* 96.5, pp. 585–603. DOI: 10.1002/zamm.201400231. URL: https://hal.inria.fr/hal-01235240.

[SW Mod.] Acary, V., *rock_protection_wall.py* Apr. 4, 2024Inria. LIC: Apache-2.0. SWHID: ⟨swh:1:cnt:ade5eb54939407f058dbaaec28ff285b5e71ba86;origin=https://gricad-gitlab.univ-grenoble-alpes.fr/nonsmooth/siconos-tutorials;visit=swh:1:snp:a2682a0bb31f68fd424b93a489b7b171cbeb0340;anchor=swh:1:rev:a04ed23ceb61f4d4024ff75fe45aff7c65acbcdb;path=/examples/mechanics/Masonry/RockProtectionWall/rockprotectionwall.py⟩.

Acary, V., M. Brémond, and O. Huber (2018). "Advanced Topics in Nonsmooth Dynamics." In: Acary, V., Brüls. O., and Leine, R. (eds). Springer Verlag. Chap. On solving frictional contact problems: formulations and comparisons of numerical methods.

Acary, V. et al. (Feb. 2011). "A formulation of the linear discrete Coulomb friction problem via convex optimization". In: *Journal of Applied Mathematics and Mechanics / Zeitschrift für Angewandte Mathematik und Mechanik* 91.2, pp. 155–175. DOI: 10.1002/zamm.201000073. URL: https://inria.hal.science/inria-00495734.

Acary, V. et al. (2019). *An Introduction to Siconos*. Grenoble: INRIA.

Acary, V. et al. (Apr. 2023). "Second order cone programming for frictional contact mechanics using interior point algorithm". working paper or preprint. URL: https://hal.science/hal-03913568.

Ahrens, J., B. Geveci, and C. Law (2005). "36 - ParaView: An End-User Tool for Large-Data Visualization". In: *Visualization Handbook*. Ed. by C.D. Hansen and C.R. Johnson. Burlington: Butterworth-Heinemann, pp. 717–731. ISBN: 978-0-12-387582-2. DOI: https://doi.org/10.1016/B978-012387582-2/50038-1. URL: https://www.sciencedirect.com/science/article/pii/B9780123875822500381.

Barquins, M. (Aug. 1, 1985). "Sliding Friction of Rubber and Schallamach Waves — A Review". In: *Materials Science and Engineering* 73, pp. 45–63. ISSN: 0025-5416. DOI: 10.1016/0025-5416(85)90295-2. URL: https://www.sciencedirect.com/science/article/pii/0025541685902952.

Berman, N., G. Cohen, and J. Fineberg (2020). "Dynamics and Properties of the Cohesive Zone in Rapid Fracture and Friction". In: *Physical Review Letters* 125.12, p. 125503. ISSN: 10797114. DOI: 10.1103/PhysRevLett.125.125503. pmid: 33016754. URL: https://doi.org/10.1103/PhysRevLett.125.125503.

Capobianco, G. and S.R. Eugster (2018). "Time Finite Element Based Moreau-type Integrators". In: *International Journal for Numerical Methods in Engineering* 114.3, pp. 215–231. ISSN: 1097-0207. DOI: 10.1002/nme.5741. URL: https://onlinelibrary.wiley.com/doi/abs/10.1002/nme.5741.

Cholet, C. (1998). "Chocs de solides rigides". PhD thesis. Paris 6.

Collins-Craft, N. A., F. Bourrier, and V. Acary (2024). *On the Formulation and Implementation of Mixed Mode I and Mode II Extrinsic Cohesive Zone Models with Contact and Friction*. URL: https://hal.science/hal-04447397. preprint.

[SW] Coumans, E. and Y. Bai, *PyBullet, a Python module for physics simulation for games, robotics and machine learning* 2016–2021. URL: http://pybullet.org.

Fetecau, R.C. et al. (Aug. 23, 2003). "Nonsmooth Lagrangian Mechanics and Variational Collision Integrators". In: *SIAM Journal on Applied Dynamical Systems* 2.3, pp. 381–416. DOI: 10.1137/S1111111102406038. URL: https://epubs.siam.org/doi/epdf/10.1137/S1111111102406038.

Frémond, M. (1995). "Rigid bodies collisions". In: *Physics Letters A* 204.1, pp. 33–41.

— (2001). "Internal constraints in mechanics". In: *Philosophical Transactions of the Royal Society of London. Series A: Mathematical, Physical and Engineering Sciences* 359.1789, pp. 2309–2326.

— (2002). *Non-Smooth Thermomechanics*. Springer Berlin Heidelberg. DOI: 10.1007/978-3-662-04800-9. URL: https://doi.org/10.1007%2F978-3-662-04800-9.

— (2007). *Collisions*. Universita di Roma Tor Vergata - Dip Ing. Civile.

— (2017). "The Theory: Mechanics. An Example: Collision of a Point and a Plane". In: *Collisions Engineering: Theory and Applications*, pp. 5–32.

Geuzaine, C. and J.-F. Remacle (Sept. 10, 2009). "Gmsh: A 3-D Finite Element Mesh Generator with Built-in Pre- and Post-Processing Facilities". In: *International Journal for Numerical Methods in Engineering* 79.11, pp. 1309–1331. ISSN: 00295981. DOI: 10.1002/nme.2579. URL: http://doi.wiley.com/10.1002/nme.2579.

Glocker, C. (2013). "Energetic consistency conditions for standard impacts: Part I: Newton-type inequality impact laws and Kane's example". In: *Multibody System Dynamics* 29.1, pp. 77–117. DOI: 10.1007/s11044-012-9316-9.

Jean, M. (1999). "The non-smooth contact dynamics method". In: *Computer Methods in Applied Mechanics and Engineering* 177. Ed. by J.A.C. Martins and A. Klarbring. Special issue on computational modeling of contact and friction, J.A.C. Martins and A. Klarbring, editors, pp. 235–257.

Jean, M. and J.J. Moreau (1987). "Dynamics in the presence of unilateral contacts and dry friction: a numerical approach". In: *Unilateral problems in structural analysis. II*. Ed. by G. Del Pietro and F. Maceri. Wien: CISM 304, Spinger Verlag, pp. 151–196.

Johnson, G., S. Leyendecker, and M. Ortiz (2014). "Discontinuous Variational Time Integrators for Complex Multibody Collisions". In: *International Journal for Numerical Methods in Engineering* 100.12, pp. 871–913. ISSN: 1097-0207. DOI: 10.1002/nme.4764. URL: https://onlinelibrary.wiley.com/doi/abs/10.1002/nme.4764.

Jourdan, F., P. Alart, and M. Jean (Mar. 1998). "A Gauss–Seidel like Algorithm to Solve Frictional Contact Problems". In: *Computer Methods in Applied Mechanics and Engineering* 155.1, pp. 31–47. ISSN: 0045-7825. DOI: 10.1016/S0045-7825(97)00137-0. URL: https://www.sciencedirect.com/science/article/pii/S0045782597001370.

Kane, T.R. (1984). "A dynamics puzzle". In: *Stanford Mechanics Alumni Club Newsletter* 6, pp. 1–4.

Leine, R. and N. van de Wouw (2008). *Stability and Convergence of Mechanical Systems with Unilateral Constraints*. Vol. 36. Lecture Notes in Applied and Computational Mechanics. Springer Verlag.

Lozano, R. et al. (2013). *Dissipative systems analysis and control: theory and applications*. Springer Science & Business Media.

Moreau, J.J. (1971). "Sur l'évolution d'un système élasto-visco-plastique". In: *Comptes rendus hebdomadaires des séances de l'Académie des sciences* 273, pp. 118–121. URL: https://hal.archives-ouvertes.fr/hal-01868142.

— (1973). "On Unilateral Constraints, Friction and Plasticity". In: *New Variational Techniques in Mathematical Physics*. Ed. by G. Capriz and G. Stampacchia. Springer. URL: https://hal.archives-ouvertes.fr/hal-01793413.

— (1988). "Unilateral contact and dry friction in finite freedom dynamics". In: *Nonsmooth Mechanics and Applications*. Ed. by J.J. Moreau and Panagiotopoulos P.D. CISM, Courses and lectures 302. Wien: CISM 302, Springer Verlag, pp. 1–82.

Puso, M.A., J.H. Porter, and T. Slavik (2024). "Structure Preserving and Energy Dissipative Contact Approaches for Implicit Dynamics". In: *International Journal for Numerical Methods in Engineering* n/a.n/a, e7454. ISSN: 1097-0207. DOI: 10.1002/nme.7454. URL: https://onlinelibrary.wiley.com/doi/abs/10.1002/nme.7454.

Schallamach, A. (Apr. 1, 1971). "How Does Rubber Slide?" In: *Wear* 17.4, pp. 301–312. ISSN: 0043-1648. DOI: 10.1016/0043-1648(71)90033-0. URL: https://www.sciencedirect.com/science/article/pii/0043164871900330.

[SW] Schlömer, N., *meshio: Tools for mesh files* 2022. LIC: MIT. DOI: 10.5281/zenodo.1173115, URL: https://github.com/nschloe/meshio, SWHID: ⟨swh:1:dir:6e1cd14ba43f09c1e729f41f4b6e2ad5fb0d6c24;origin=https://github.com/nschloe/meshio;visit=swh:1:snp:9d55efa5b1f7ff0238d8557c5aee1673b55e3d29;anchor=swh:1:rev:b2ee99842e119901349fdeee06b5bf61e01f450a⟩.

Viswanathan, K. and S. Chandrasekar (Aug. 2022). "Fifty Years of Schallamach Waves: From Rubber Friction to Nanoscale Fracture". In: *Philosophical Transactions of the Royal Society A: Mathematical, Physical and Engineering Sciences* 380.2232, p. 20210339. DOI: 10.1098/rsta.2021.0339. URL: https://royalsocietypublishing.org/doi/10.1098/rsta.2021.0339.